CENTENNIAL FEATURE ARTICLE

Nonlinear Optical Response and Ultrafast Dynamics in C_{60}

G. P. Zhang[†]

Department of Physics, Indiana State University, Terre Haute, Indiana 47809

X. Sun

Department of Physics, Fudan University, Shanghai 200433, China

Thomas F. George*[,‡]

Office of the Chancellor and Center for Nanoscience, Departments of Chemistry & Biochemistry and Physics & Astronomy, University of Missouri-St. Louis, St. Louis, Missouri 63121

Received: March 14, 2008; Revised Manuscript Received: December 4, 2008

C_{60} is a symbol of nanoscience. Its impact is far beyond the initial interest in this nanometer molecule itself. This paper reviews the current status of the nonlinear optical and ultrafast dynamics investigations of C_{60}. The review starts with the nonlinear optical response, in particular the dispersion spectra of harmonic generation and two-photon absorption. Both the experimental and theoretical challenges are highlighted. The main focus is on femtosecond and picosecond degenerate and nondegenerate four-wave mixing and pump-probe techniques as a tool to investigate ultrafast electron and nuclear dynamics, charge transfer and photoexcitation in C_{60}. Theoretical investigations are essential to understand these processes. Theory predicts a longer relaxation time for charge transfer than photoexcitation and reveals the underlying reasons for the normal mode excitations and changes in the electron density of states, which is directly linked to the time-resolved photoemission spectra. Theory also resolves a long-time puzzle about the dependence of normal mode excitations on the laser pulse duration and predicts that time-resolved pump-probe spectroscopy is able to probe electron correlation effects. Finally, high-harmonic generation in C_{60} is reviewed. The review concludes with prospectives and possible applications.

I. Introduction

When light impinges on a medium, it excites the electrons and nuclei and induces an optical response. If the laser field is weak, then the response is linear with the light field, i.e., a linear response. A nonlinear optical response refers to a process where the output signal is proportional to the light field superlinearly, and output frequencies can be doubled or tripled with respect to that of the incident light.[1,2] One example is the green laser pointer, where a nonlinear optical crystal (normally potassium titanyl phosphate or KTP, $KTiOPO_4$) converts red light into green light. However, to generate a strong nonlinear optical signal is a major challenge both experimentally and theoretically, as it requires strong light such as a laser and a highly nonlinear optical medium. Metallic systems are not a suitable medium since the electron screening effect is too strong. The major materials are semiconductors.[3] Organic molecules in general and conjugated polymers in particular are very attractive in this respect,[4] as they exhibit a strong nonlinear response. Polyacetylene (PA) and polydiacetylene (PDA) are among those most frequently investigated for the third-order nonlinear optical response. In PA, the charge dynamics, upon laser excitation, is extremely fast, on the order of several hundred femtosecond, with formation of self-trapped polarons. This fast response is a good indication of large optical nonlinearity.

For quasi-one-dimensional materials, if the electron correlation is weak, the third-order response is proportional to E_g^{-6}, where E_g is the energy gap.[5−12] Therefore, searching for those materials with smaller band gaps is a good strategy. Unfortunately, there is no generic design formula to follow if the electron correlation is strong and the material is no longer one-dimensional. The challenge mainly results from the fact that both ground and excited states affect nonlinear optical processes. Nevertheless, the ever-growing demand for nonlinear optical materials has motivated active investigations for over two decades. Inorganic materials such as $LiNbO_3$ (for telecommunications), KTP, potassium dihydrogen phosphate (KH_2PO_4) or KDP, β-barium borate (β-BaB_2O_4) or BBO and others (for electrooptical and laser applications) take the lion's share.[13] While these materials involve mainly second-order processes, organic materials such as PA, PDA, and guest-host and chromophore-attached polymeric films are promising for both second- and third-order nonlinear optical processes.[14−16]

It is appropriate to review some of the basic concepts in nonlinear optics. Under the influence of a laser field, the polarization of a medium can be expanded in terms of the laser's electric field $\mathbf{E}(\mathbf{r}, t)$ as[17]

* To whom correspondence should be addressed.
[†] E-mail: gpzhang@indstate.edu.
[‡] E-mail: tfgeorge@umsl.edu.

10.1021/jp802244b CCC: $40.75 © 2009 American Chemical Society
Published on Web 01/26/2009

Guoping Zhang is an assistant professor of physics at Indiana State University (ISU) and starts his associate professor position in fall 2008. Before joining ISU, he had a one year appointment as a visiting assistant professor at Buffalo State College and two postdoctoral appointments: one at the Max Planck Institute for Microstructure Physics in Germany and the other at the University of Tennessee at Knoxville. He obtained his Ph.D. from Fudan University in Shanghai, China. His research interests includes ultrafast spectroscopy, nanostructures, fullerenes, femtomagnetism, spintronics, nonlinear optics, strongly-correlated electron systems, pump-probe and four-wave mixing signal, ultrafast spin dynamics in nano- and low-dimensional magnets, soft X-ray spectroscopy, high harmonic generation, mechanical properties of diamondoids, superconductivity in MgB_2, and photoisomerization in rhodopsin. He is a Promising Scholar at ISU.

Xin Sun is a professor of physics at Fudan University in Shanghai, China. From 1978 to 1979, he was associate professor of physics. From 1989 to 1992, he was a guest scientist at the International Center for Theoretical Physics in Trieste, Italy. From 1990 to 1991, he was a visiting professor at the National Institute for Molecular Science in Okazaki, Japan. In 1993, he was a visiting professor at the University of Alberta in Canada. His research fields are in the theory of condensed matter physics, especially in conducting polymers, organic nonlinear optical materials, fullerenes, metal surfaces, superconductivity, ferromagnetism, many body theory with the correlated basis-function method, phase transitions, and critical phenomena. He has won an award from the National Science Foundation and an award from the National Science of Academic Sinica.

$$\mathbf{P}(\mathbf{r},t) = \chi^{(1)} \cdot \mathbf{E}(\mathbf{r},t) + \chi^{(2)} : \mathbf{E}(\mathbf{r},t)\mathbf{E}(\mathbf{r},t) + \chi^{(3)} : \mathbf{E}(\mathbf{r},t)\mathbf{E}(\mathbf{r},t)\mathbf{E}(\mathbf{r},t) + \ldots \quad (1)$$

where $\chi^{(1)}$ is the first-order or linear susceptibility and $\chi^{(2)}$ and $\chi^{(3)}$ are the second- and third-order susceptibilities, respectively. In eq 1 the same $\mathbf{E}(\mathbf{r},t)$ is used, but in practice, they can be different or the same, depending on whether one or multiple laser pulses are used. $\mathbf{E}(\mathbf{r},t)$ can be a continuum wave (cw) or a short pulse. In general, all of the susceptibilities are tensors, and in eq 1, we use different dots to highlight this feature. The susceptibility depends on the symmetry of a system. For a system with inversion symmetry, $\chi^{(2)} = 0$, it can become nonzero if the inversion is broken, such as on surfaces or if the magnetic

Thomas F. George is chancellor and professor of chemistry and physics at the University of Missouri-St. Louis. Born in Philadelphia (1947), he received his B.A. degree (1967) in chemistry and mathematics from Gettysburg College and M.S. and Ph.D. degrees (1968 and 1970) in theoretical chemistry from Yale University, followed by postdoctoral appointments at MIT and UC, Berkeley. His research interests are in chemical/materials/laser/nanophysics. His work has led to nearly 700 papers, 5 authored textbooks, 15 edited books/volumes, and over 200 conference abstracts. His international honors include the Marlow Medal and Prize from the Royal Society of Chemistry in Great Britain, election to the Korean Academy of Science and Technology, and most recently in 2008, an honorary doctorate in physics (honoris causa) from the University of Szeged in Hungary. He is a fellow of the NY Academy of Sciences, APS, SPIE, and AAAS and has been a Sloan fellow and Dreyfus fellow. He has been active in the American Chemical Society, such as serving as chair of the Physical Division, organizing symposia at national meetings, and editing books in the ACS Symposia Series.

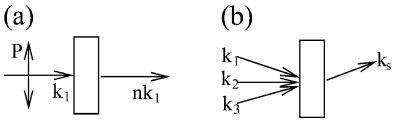

Figure 1. (a) Typical nonlinear optical process. Here, only one wave is incident on the sample. The signal is just along the original incident direction, with the wavevector as a multiple of the incident one. (b) Three-wave process. Three waves with wavevectors of $\vec{k}_1$, $\vec{k}_2$, and $\vec{k}_3$ radiate the sample, and a signal wave $\vec{k}_s$ is emitted. See all of the possible combinations in the text.

contribution is included. The third-order susceptibility $\chi^{(3)}$ has four indices to identify the laser polarization directions. The first three indices identify the incoming laser polarizations, and the fourth identifies the outgoing light polarization. Since each index has three possible directions (see Figure 1a), x, y and z, there are $3^4 = 81$ terms in total, but the larger ones normally have all four polarization directions along the same direction.

A complication arises since the laser not only has a specific polarization direction but also has a wave vector $\vec{k}$ to identify the wave propagation direction. Experimentally, only a few propagation directions are probed. Figure 1b shows one example for the third-order process. If the incident light consists of three wavevectors $\vec{k}_1$, $\vec{k}_2$, and $\vec{k}_3$ and three frequencies ω_1, ω_2, and ω_3, the signal will propagate along any of these directions [$\pm\vec{k}_1$ $\pm\vec{k}_2$ $\pm\vec{k}_3$], with their respective signal frequencies [$\pm\omega_1$ $\pm\omega_2$ $\pm\omega_3$]. If one wants to probe the harmonic generation, then one should probe the signal along the direction $\vec{k}_s = \vec{k}_1 + \vec{k}_2 + \vec{k}_3$. For four-wave mixing, one probes signals along the directions $\vec{k}_1 + \vec{k}_2 - \vec{k}_3$, $\vec{k}_1 - \vec{k}_2 + \vec{k}_3$ and $-\vec{k}_1 + \vec{k}_2 + \vec{k}_3$. In degenerate four-wave mixing (DFWM), all four frequencies are the same. It is clear that all χ must carry these extra $\vec{k}$ indices, which is the case for X-ray pulses. For visible light, if the pulse wavelength is much larger than the system dimension and the dipole approximation is valid, the $\vec{k}$ indices can be dropped. However, there is an exception. When a specific direction is

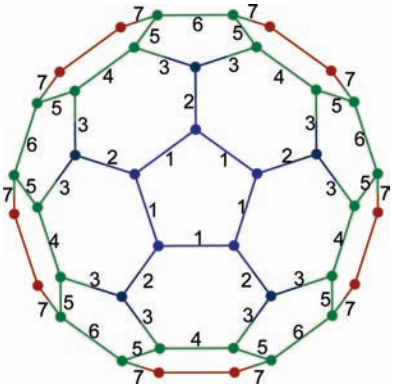

Figure 2. C_{60} structure viewed along the z axis. The numbered layers of the equivalent bonds start from the front to the back of the buckyball. The front layer, the center pentagon, is number 1; the bottom layer, not shown but opposite the center pentagon, is number 13.

needed within the dipole approximation, this requires a special treatment to identify those directions (see section IV.D).

The discovery of C_{60},[18] fullerene, opened a new era for nanoscience and nonlinear optics. This sixty carbon-atom buckyball is similar to a soccerball (see Figure 2) and has inspired intense nanoscience research. Such a structure allows large charge (π electron) conjugation (delocalization), which is essential to its fast response time and large nonlinear optical effect. Depending on the type of laser used, earlier studies can be roughly categorized into two groups. The first group uses a pulse laser, with the pulse duration varying from a few nanoseconds (YAG laser) to a few tens of femtosecond (Ti-sapphire laser), and with one or two different wavelengths. Although most of the lasers had only one wavelength and relied on the picosecond YAG laser, with signals that are nearly featureless, they are useful to extract the magnitude of the nonlinear optical response and pave the way for the investigation of femtosecond dynamics. An early study showed a huge nonlinear response[19] but was disputed by Kafafi et al.[20,21] and Knize and Partanen.[22] In 1991, Hoshi et al.[23] used a Nd:YAG laser to study the second- and third-harmonic generation in C_{60} thin films and found a third-order response of 2×10^{-10} esu. In 1992, Tutt and Kost[24] used 8-ns pulses to investigate the optical limiting effect in C_{60}, with saturation thresholds comparable to or lower than existing materials, which was also found in new fullerene derivatives.[25,26] McLean et al.[27] used 532-nm and 8-ns and 30-ps laser pulses to further study the fluence dependence in a C_{60}-toluene solution.[28] Its potential impact has been recently reviewed by Huo et al.[29] and Martin et al.[30] In 1997, Rustagi et al.[31] presented a detailed review of nonlinear optical properties of fullerenes. In the same year, Belousov et al.[32] summarized photodynamics in fullerene-containing materials and nonlinear susceptibility in fullerenes and harmonic generation in both C_{60} and C_{70}. The reader may find a book on this topic useful.[33]

The second group uses multiple wavelengths and is able to measure the whole dispersion spectrum of the second- or third-order processes. We will postpone a discussion of this to section II, where we give an extensive survey (some representative experiments[19−21,34−44] are listed in Table 1). Bendikov, Wudl, and Perepichka[45] reviewed the possibility of using fullerene as an acceptor for donor-acceptor diads. A joint experimental and theoretical investigation was carried out by Xenogiannopoulou et al.[46] to show that all fullerene dyads studied exhibit enhancement of their NLO response compared to pristine fullerenes. In 2008, Mateo-Alonso et al.[47] revealed an efficient modulation of the third-order nonlinear optical properties of fullerene derivatives. Many of the recent investigations have focused on fullerene-derivatives.[48−50]

This present review provides a survey of some of the major experimental and theoretical developments in this field and points out a few areas that need attention. Due to our own interest, we emphasize the nonlinear optical response and, in particular, laser-induced dynamics, both of which have received considerable attention. We do not attempt to cover the fragmentation of C_{60}, as it has been reviewed recently elsewhere.[51] We refer the reader to other excellent reviews[52,53] for other properties.

The paper is arranged as follows. Section II introduces some important measurements and calculations of the spectral dispersions of the third-order harmonic generations and two-photon absorption spectra in C_{60}. These reflect some of the achievements in this field. Section III is devoted to ultrafast dynamics, where the focus is the picosecond and femtosecond time domains. Theoretical investigations are presented in section IV, followed by prospectives and possible applications in section V.

II. Harmonic Generation, Two-Photon Absorption, and Four-Wave Mixing

C_{60} has a cage structure with I_h symmetry, where the carbon atoms are situated at the corners of a truncated icosahedron (see Figure 2). The double and single bond lengths are 1.40 and 1.46 Å, and the diameter is about 7.1 Å. All of the carbon atoms are equivalent. In total, there are 120 symmetry operations. We number the bond layers from the front to the back, with the center front pentagon being layer 1 and the back pentagon (not shown) layer 13. Electronically, the bonds are sp^2-sp^3 hybridized; the energy gap is 2.0 eV. A large charge conjugation, expected from this structure, underlies its fast optical response.

Nonlinear optical investigations started almost immediately after the discovery of C_{60}. These earlier studies were mainly single-wavelength measurements,[37,54] but they laid a solid groundwork for future investigations. No complete dispersion of the third-order optical nonlinearity was available until 1992, when Meth et al.[38] succeeded in measuring such a comprehensive dispersion in a polycrystalline sample. Figure 3 shows that the three-photon resonance peaks at $\hbar\omega = 0.94$ eV, which corresponds to the 2.8 eV dipole-allowed transition ($\hbar\omega$ refers to the fundamental laser energy). The off-resonant value at $\hbar\omega = 0.52$ eV is $|\chi^{(3)}(-3\omega; \omega, \omega, \omega)| = (4.1 \pm 0.6) \times 10^{-12}$ esu, whereas at $\hbar\omega = 0.94$ eV, $|\chi^{(3)}(-3\omega; \omega, \omega, \omega)| = (2.7 \pm 0.4) \times 10^{-11}$ esu. However, to get an objective measure, one has to compute the ratio of $|\chi^{(3)}|$ to the absorption coefficient α, since if the absorption is too strong, the third-order harmonic signal will be weak. The ratio $\chi^{(3)}/\alpha$ at $\hbar\omega = 0.52$ eV is 0.205 (esu/μm^{-1}) is almost same as 0.208 (esu/μm^{-1}) at $\hbar\omega = 0.94$ eV. This proves to be a fairly sizable value of the third-order harmonic generation in C_{60}. Two years later, Kajzar et al. reported two resonant peaks. One resonant peak is at the fundamental wavelength of 1.323 μm (or 441 nm harmonic wavelength, i.e., a third because it is a third-order process),[39] with $\chi^{(3)}(-3\omega; \omega, \omega, \omega) = 6.1 \times 10^{-11}$ esu. This harmonic wavelength corresponds to 2.81 eV, which would be consistent with the resonant peak position in Meth's experiment, but they assigned it to a two-photon resonance with the T_{1g} forbidden state. In addition, they found a new and stronger peak at fundamental wavelength of 1.064 μm, corresponding to the 355 nm harmonic wavelength or 3.5 eV. This peak was interpreted as a three-photon resonant peak due to the dipole-allowed transition to T_{1u} state. In 1997, the wave-dispersed two-photon

TABLE 1: Experimental Nonlinear Optical Response from Pure C_{60} Thin Films or C_{60} in Solution or Matrix[a]

method	year	authors	laser pulse	form	χ^3 (esu)	uncertainty	ref
DFWM	1991	Blau et al.	50 ps/1064 nm	benzene	6×10^{-8}	4×10^{-8}	19
DFWM	1992	Kafafi et al.	35 ps/1064 nm	film/toluene	7×10^{-12}	NA	20, 21
DFWM	1992	Talapatra et al.	400 fs/602 nm	benzene	2.2×10^{-10}	0.3×10^{-10}	43
DFWM	1992	Gong et al.	NA/1064 nm	toluene	3.3×10^{-9}	NA	34
DFWM	1993	Lindle et al.	35 ps/1064 nm	film	7×10^{-12}	NA	35
DFWM	1997	Strohkendl et al.	100 fs/variable	film	dispersion	NA	36
THG	1991	Hoshi et al.	NA/1064 nm	film	2×10^{-10}	NA	23
THG	1992	Neher et al.	10 ns/1064,1500,2000 nm	film	NA	NA	37
THG	1992	Meth et al.	variable	film	dispersion	variable	38
THG	1994	Kajzar et al.	variable	film	dispersion	NA	39
TPA	1994	Bezel et al.	300 fs/612 nm	film	2.6×10^{-11}	1.3×10^{-11}	41
TPA	1997	Banfi et al.	variable	film	dispersion	NA	40
TPA	2004	Yamaguchi et al.	variable	toluene	dispersion	NA	42
PP	1991	Dexheimer et al.	12 fs/620 nm	film	NA	NA	44

[a] DFWM refers to degenerate four wave mixing; THG to third harmonic generation; TPA to two-photon absorption; and PP to pump-probe experiment.

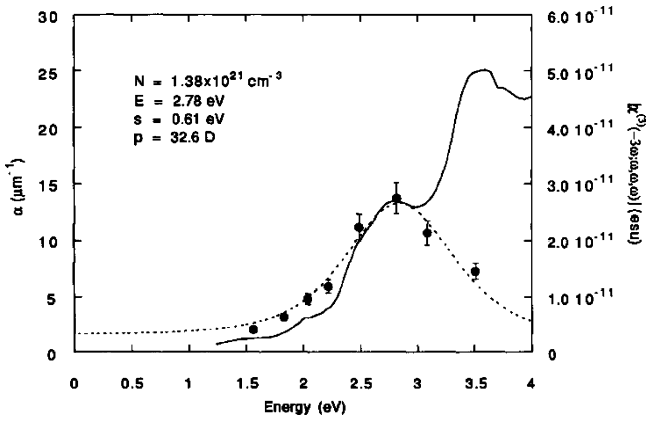

Figure 3. Linear absorption (solid line) and dispersion of the third-order harmonic generation $|\chi^{(3)}(-3\omega; \omega, \omega, \omega)|$ (filled circles) of C_{60}.[38] The parameters in the inset are obtained by fitting to a two-level model. The transition moment $P = 32.6$ D in the figure should be 9 D due to an error in one of the formulas (communication from Jeff Meth). Courtesy of Jeff Meth and Ying Wang.

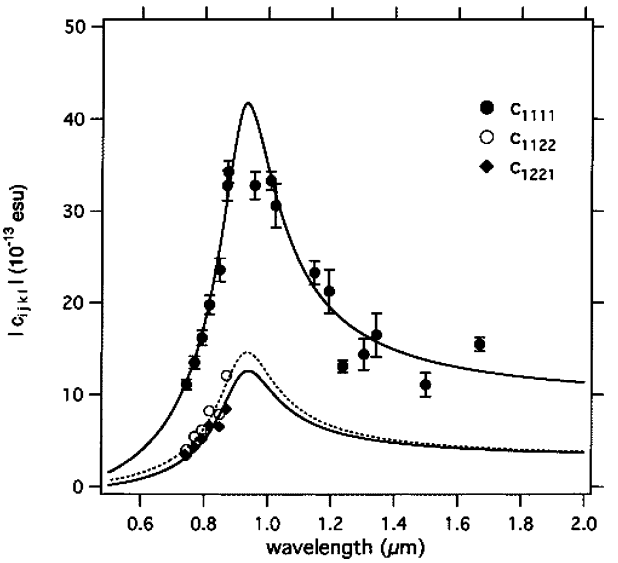

Figure 4. Degenerate four-wave mixing for several different components as a function of wavelength in a C_{60} thin film.[36] Courtesy of Robert Hellwarth.

absorption $\chi^{(3)}(-\omega; \omega, -\omega, \omega)$ was measured by Banfi et al. in a polycrystalline C_{60} film.[40] The spectrum shows two maxima, one at 2.58 eV and the other at 3.5 eV. It would be interesting to have a direct comparison between these two 3.5 eV peaks, as it may contain detailed information about the electronic structures.

Strohkendl et al.[36] reported several very detailed femtosecond (pulse duration about 100 fs) degenerate four-wave mixing dispersion measurements $[\chi^{(3)}(-\omega; \omega, \omega, -\omega)]$ for a wavelength between 0.74 and 1.70 μm. One of their key results is shown in Figure 4. The data show a single peak at 0.93 μm, which was assigned to a two-photon resonance between the ground-state and excited state H_g. Drenser et al.[55] presented a brief review on degenerate four-wave mixing experiments up to 1999. In 2004, using nondegenerate two-photon absorption spectroscopy, Yamaguchi and Tahara[42] found another optical forbidden state at 314 nm, but could not reproduce the above 0.93 μm peak by Strohkendl. The reason for this discrepancy is still unknown.

Theoretical investigations followed the experimental studies pretty closely. However, calculations generally have been very difficult since one deals with such a large system and must compute the excited states with high accuracy. This remains true even today. In 1992, Shuai and Bredas used the valence-effective Hamiltonian to compute third-order harmonic generation and four-wave mixing spectra, finding good consistency.[56] Quong and Pederson computed the static hyperpolarizability but did not address the dispersion spectrum.[57] Matsuzawat and Dixon[58] used the local density functional method and found a second-order hyperpolarizability of 15.9×10^{-36} esu, which is much lower than the experimental values. In 1993, Takahashi et al.[59] used the time-dependent Hartree-Fock approximation to investigate collective charge fluctuations and linear and nonlinear optics responses. The calculation relied on the equation of motion of the density matrix. While their calculation was fully dynamical in principle, they Fourier-transformed their results to the frequency domain. Li et al.[60] used both the INDO/SCI and INDO/SDCI methods and the sum-overstates scheme to compute the third-order optical susceptibility. Their computed values were $\gamma(-\omega; \omega, -\omega, \omega) = 7.30 \times 10^{-34}$ esu at $\lambda = 1.064$ μm and $\gamma(-2\omega; \omega, \omega, 0) = 6.90 \times 10^{-34}$ esu at $\lambda = 1.91$ μm. Westin and Rosen[61] used the local density approximation and found in general that the calculated third-order optical nonlinearity was in agreement with the experiment,[38] but the details are very different. For instance, the first resonant peak at 2.72 eV is due to the two-photon transition between HOMO and LUMO, not the dipole-allowed three-photon transition.[38] As a result, the lowest energy peaks in $\chi^{(1)}$ and $\chi^{(3)}$ do not match, a finding that is consistent with the theoretical results by Harigaya and Abe.[62] We note Meth et al.[38] assigned their peak at 2.8 eV

to a three-photon transition. It is possible that there is an overlap in this region. In 1995, within the semiempirical CNDO/S approximation, using single and double configuration interaction methods, Hara et al.[63] computed the hyperpolarizability and found that it is essential to include both single and double excitation configurations, and the theoretical results agree with the experimental ones better for the off-resonance wavelengths. Fanti et al.[64] performed a semiempirical investigation at the sum-overstates and CNDO/SCI level for a group of carbon clusters. They found that their results are in good agreement with the experimental results for C_{60} and C_{70}, but their main peak position appears around 870 nm, while the experimental first peak is at 1.06 μm.

Bechstedt et al. performed a configuration interaction calculation within a model Hamiltonian and assigned the 3.5 eV peak to the T_{1u} exciton,[65] which is consistent with the experimental assignment, and the 1.9 eV peak to the H_g exciton. Most later theoretical studies did not address this issue explicitly. For instance, van Gisbergen et al. instead tried to obtain an accurate result at a low-frequency limit via the finite field element method,[66] with a similar study done by Nomura et al.,[67] Iwata et al.,[68] and Norman et al.[69] A time-dependent density functional theory (DFT) calculation was used to compute the second-order hyperpolarizability, yielding results quite different from the experimental ones.[70] This is not surprising, since it may reflect the fundamental difficulties in DFT for the excited states. In 2004, Zhou et al.[71] used the ZINDO method to compute the two-photon absorption spectrum and found a single peak at 518 nm (2.4 eV). In 2005, Jensen et al.,[72] using the discrete solvent reaction field model, and combining the time-dependent density functional theory, computed THG and degenerate four-wave mixing (DFWM) in the condensed phase. The agreement with THG experiments was within a factor of 2 but worse for DFWM. Their emphasis was on the zero- and small-frequency region, and no full dispersion across these resonant regions was computed. Therefore, further theoretical investigations are needed to clarify these complex issues. We should mention that enhancements of the third-order nonlinear optical response in excited states of C_{60} were investigated by Cheng et al.[73]

III. Experimental Investigation of Ultrafast Dynamics

Investigations of ultrafast dynamics have been very encouraging, as they may lay the groundwork for future applications such as solar energy conversion.[30] The emphasis is on laser excitation and charge transfer.[74−80] Although most earlier experiments used picosecond or nanosecond lasers, they did provide important insight into photoinduced charge transfer. In 1991, Sension et al.[81] investigated transient charge transfer with *N*,*N*-dimethylaniline (DMA) and demonstrated formation of the DMA+:C_{60}-ion pair on a time scale of about 1−2 ps. Dexheimer et al.[44] employed a pump-probe technique with the then-shortest 12 fs pulse centered at 620 nm to excite two A_g modes (radial breathing mode and pentagonal pinching mode). Figure 5 shows the differential transmittance change as a function of time delay between pump and probe pulses. This experiment represents the first femtosecond investigation into an ultrafast dynamics investigation of C_{60}.

In addition to the pump-probe experiments, several DFWM measurements were reported. In 1992, Kafafi et al.[21] used a 35 ps Nd:YAG laser (1.064 μm) to find an off-resonant third-order susceptibility $\chi^{(3)}_{xxxx} = 7 \times 10^{-12}$ esu and discovered the fifth-order contribution by fitting the nonlinear signal as a function of intensity. Ryasnyansky et al.[82] recently showed there is a competition between third- and fifth-order nonlinear optical processes in C_{60} thin films. Talapatra et al.[43] performed a DFWM experiment (400 fs pulse) and optical Kerr gate experiment (60 fs pulse) at a wavelength of 602 nm. The second-order complex hyperpolarizability was found to be $[-(5 \pm 2) + i(9 \pm 1)] \times 10^{-33}$ esu, but their theoretical results are 3 orders of magnitude smaller. In 1993, Kraabel et al. reported that photoinduced electron transfer occurs in less than 1 ps between C_{60} and conducting polymers.[83] In 1994, Thomas et al.[84] measured the forbidden transition between the highest occupied molecular orbital (HOMO) and lowest unoccupied molecular orbital (LUMO). This is a very significant study, since it may directly access the excitonic excitation which is coupled by the vibrational excitation. However, their study only used one energy (610 nm or 2.03 eV). A scan of laser energy across the band gap is necessary.

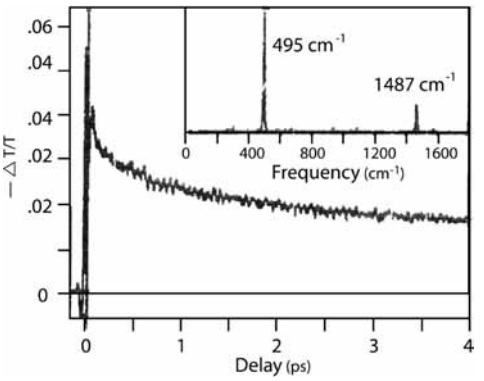

Figure 5. Differential transmittance change with the time delay between pump and probe beams.[44] The pulse duration is 12 fs. The inset shows the Fourier transformed results, with the first peak corresponding to the $A_g(1)$ mode and the second to the $A_g(2)$ mode. The intensity of the $A_g(1)$ mode is higher. Note these two modes are not Jahn-Teller active, so that their frequency changes due to the relaxation are very small. Courtesy of S. L. Dexheimer.

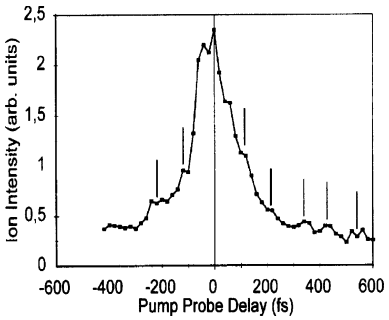

Figure 6. Ion intensity as a function of time delay between pump and probe pulses. Both pulses have the wavelength of 620 nm. The pump pulse has intensity 30 μJ and the probe 20 μJ. An obvious oscillation is observed, which is assigned to $H_g(1)$ (courtesy of I.V. Hertel).[85]

In 1994, Hohmann et al.[85] used two different kinds of laser pulses, 15 ns and 100 fs, to study the photoionization and fragmentation dynamics of C_{60}. The initial fragmentation starts with fragments larger than C_2. An oscillatory behavior was observed in the ion intensity (see Figure 6), which they assigned to the phonon $H_g(1)$ mode oscillation. To our knowledge, this is the first experiment that demonstrated the H_g excitation in time-resolved photoemission. The experiment reveals new insight into the ionization mechanism, and their observations can be directly compared with theoretical results (see below). Bezel et al.[41] conducted irradiance-dependent transmission measurements for a thin C_{60} film using a 300 fs laser pulse of 612 nm. They conclude from the upper limit for the two-photon absorption coefficient that $Im\chi^{(3)}$ is $(2.6 \pm 1.3) \times 10^{-11}$ esu.

Yang et al.[86] performed time-resolved degenerate four-wave mixing at 532 nm in C_{60} in toluene solution. They found that the risetime of the four-wave mixing signal becomes shorter as the excitation energy increases. They assigned this to the larger singlet-singlet absorption cross section.

In 1995, Couris et al.[87] employed transient degenerate four-wave mixing (DFWM) and *z*-scan techniques using 0.5 ps laser pulses at 497 nm and investigated the concentration dependence of the $\chi^{(3)}$. They found the molecular second hyperpolarizability γ of C_{60} to be $(2.3 \pm 0.6) \times 10^{-32}$ esu.

In 1997, Boucher et al.[88] employed the pump-probe technique to investigate ultrafast relaxation of fullerenes and fullerites by broadband femtosecond laser spectrometry. The intensity was varied over the range $10^{10}-10^{12}$ W/cm^2, the energy from 1.57 to 3.14 eV, and the pulse duration from 60 to 350 fs. The differential absorption was used to probe both the time and energy domain information. An increase in absorption was observed in solutions with a time constant of 1.2 ps. The investigation by Farztdinov et al.[89] represents a very much needed determination of the spectral dependence of ultrafast relaxation, though their pulse duration was not as short as that of Dexheimer's.[44] Three crucial results were reported. First, the relaxation time has a minimum at 2 eV and a kink at 2.4 eV, but the time evolution shows a strong energy dependence at earlier stages, which prevents using a simple exponential fitting. They first excited the sample by a 50 fs pump pulse at two photon energies, 2.34 and 2.59 eV. Their probe pulse was a supercontinuum beam with energy over the range 1.6−3.0 eV. Both the dimerization and possible state filling effects are responsible for the distinctive relaxation processes. In particular, the H_g modes with 5-fold symmetry are substantially affected. However, no A_g mode excitation was probed. This may suggest their pulse durations are still too long.

In 1998, Ishihara et al.[90] used a colliding-pulse mode-locked ring dye laser with laser duration of 100 fs and wavelength of 628 nm and spectral broad continuum pulses (1.2−2.0 eV) as probe pulses. They estimated the decay time of the self-trapped exciton as 570 ± 120 fs and that of the polaron as 54 ± 7 ps. The huge difference between them is obvious, which agrees with the theoretical prediction.[91] Buche et al.[92] used a 60 fs pulse with wavelength of 530 nm and obtained the difference spectra as a function of time delay, which confirmed the finding by Farztdinov et al. In addition, Farztdinov et al. showed that it is possible to slow down the ultrafast relaxation process by a high 40 fs pump. The relaxation rate shows a strong energy dependence.[89]

In 1999, Sassara et al.[93] used a 2 ps laser pulse (wavelength of 450 nm) to examine the fluorence yield of C_{60}. The time-resolved fluorescence spectra reveal a wide range of normal mode excitations on a much longer time scale (larger than 30 ps). The full recovery of the fluorescence needs over 210 ps. This is a potentially interesting study. However, in order to fully examine such processes, one needs the dependence on the laser pulse duration. The electron dynamics is much faster than the lattice dynamics. Using different pulse durations isolates and extracts how strong the coupling between the electronic system and the lattice system is. Second, at least two different laser pulse energies must be used, which allows a contrast of the results to avoid potential accidental agreements.

In 2001, van Hal et al. studied a system of fullerene-oligothiophene-fullerene triad with thiophene units using sub-10 and 200 fs pump-probe spectroscopy.[94] The short pulse was a visible (500−680 nm) optical parametric amplifier based on noncollinear phase matching in β-barium borate. The long pulse was a Ti:sapphire laser of 200 fs duration and 780 nm wavelength. They found that irrespective of the polarity of the medium, the singlet-energy transfer proceeds with a time constant of 95 fs, followed by intramolecular electron transfer from the oligothiophene to the fullerene on 10 ps time scale. The ultrafast laser invoked a strong symmetric C═C stretching mode (A_g) with frequency of 1456 cm^{-1}, which belongs to thiophene. In contrast to the experiment by Dexheimer et al., normal mode vibrations of C_{60} were not observed in their experiment. It is unknown whether this is due to the wavelength dependence, since the pulse duration is short enough. Further experiments must be performed on thiophene and C_{60} separately under the same condition, with an increase in the concentration of oligothiophene to isolate two different time scales for the energy relaxation and electron transfer. Since the lattice energy relaxation must occur through the coupling between C_{60} and thiophene, a comprehensive investigation is very interesting and necessary.

In 2002, using 90 fs laser pulses, Stepanov et al.[95] measured transient absorption spectra of C_{60} molecules trapped in cryogenic rare gas matrices and dissolved in toluene. Two different wavelengths, 402 and 800 nm, were used. When the system was excited with a 402 nm laser and probed by a 800 nm one, an increase in the transient absorption as time delay between the pump and probe beams was observed. For the cross polarization of the pump and probe pulses, they found a buildup time of 200 fs, similar for C_{60} in either toluene solution or trapped in neon matrices. For the one-color absorption and parallel polarizations between the pump and probe, a coherent peak appeared, but it would be desirable to have cross-polarization results. In 2004, Bhardwaj et al.[96] used a 50-fs Ti:sapphire laser to produce a highly charged C_{60} and investigated the laser-induced dipole force on the normal mode excitation.

In 2006, Berera et al. investigated charge separation and energy transfer in a caroteno-C_{60} dyad.[97] They found that, when the dyad is dissolved in hexane, energy transfer from the carotenoid S_2 state to the fullerene takes place on a sub-100 fs time scale, and no intramolecular electron transfer was detected. Using a 15 fs pump pulse at 580 nm, Manzoni et al.[98] investigated electron transfer between 5-(3′,7′-dimethyl-octyloxy)]-*p*-phenylene vinylene (MDMO-PPV) and [6,6]phenyl C_{61} butyric acid methyl ester (PCBM). They found that the transmission is positive for the time delay between the pump and probe as less than 50 fs and becomes negative after that. They assigned the first feature to the first singlet transition and showed the second feature as charge transfer with a time constant of 65 fs.

Hertel et al.[51] have systematically investigated time-dependent ionization and fragmentation in C_{60}. By the end of the 1990s, the shortest pulse ever used to investigate the ultrafast dynamics in C_{60} was 12 fs. This record was broken by Schatsinin et al.,[99] who used a 9 fs pulse to study the ionization and fragmentation. In 2007, Laarmann et al. used a laser pulse of 27 fs duration to excite giant breathing motion in C_{60},[100] which represents an important experimental milestone in the normal mode excitation and makes a direct connection with theoretical investigations.[101] Very recently, Toivonen and Hukka theoretically investigated intermolecular resonant energy transfer of oligo(*p*-phenylenevinylene)-fullerene dyads. Their results suggest that intermolecular energy transfer can compete with intramolecular energy transfer.[102]

IV. Theoretical Study

Theoretical investigations are essential to understanding the ultrafast dynamics in C_{60}. The interests range from ultrafast laser

excitation to charge transfer and fragmentation. Jones et al.[103] recently performed an explicit time-dependent electron dynamics simulation in order to investigate nonlinear optical properties. They first computed the ground-state wave function by Gaussian 03 and transition matrix elements while freezing the nuclear motion. By solving the time-dependent Schrödinger equation, they obtained the instantaneous dipole moment change. In the following, we start with a simulation done with the dark evolution and then proceed to include the laser field explicitly. We will discuss both the electron dynamics and lattice dynamics. We predict the pump-probe technique can directly assess the electron correlation effect by measuring the quasiparticle lifetime. We will show that the laser pulse duration has a substantial effect on the normal mode excitation. C_{60} provides an example of normal mode control in larger systems. High-harmonic generation in C_{60} is a largely unexplored field. We show that there is strong harmonic generation from C_{60}, and close to the intrinsic resonance, its ellipticity dependence shows a similar anomaly as seen in atoms. This anomaly appears only if the laser field is strong enough.

A. Dark Evolution. In a laser-induced ultrafast charge-transfer process, the laser first excites an electron out of an occupied state to an unoccupied one. If the electron can overcome a potential barrier which is created by the lattice and electron, then charge transfer occurs and lattice relaxation starts. Therefore, the laser-induced charge transfer is a convoluted process. It is often necessary to address each issue separately. A frequently used method is the so-called dark evolution.

In the dark evolution method, at $t = 0$ fs, one changes the electron configuration by adding or removing or altering the electron distribution in the electronic states, and then monitors how the relaxation occurs afterward. There is no laser field included explicitly, as the name states. This technique has been used successfully for polyacetylene.[104] We start with the tight-binding Hamiltonian[91]

$$H_0 = -\sum_{ij,\sigma} t_{ij}(c^{\dagger}_{i,\sigma}c_{j,\sigma} + h.c.) + \frac{K}{2}\sum_{ij}(|\vec{r}_i - \vec{r}_j| - d_0)^2 \quad (2)$$

where (i, j) and σ are the site indices and spin index, respectively. $c^{\dagger}(c)$ is a creation (annihilation) operator, K is the spring constant, and d_0 is the nearest-neighbor distance in diamond. The summation is over the nearest-neighbors only as the next nearest-neighbor hopping is very small. Since we include one orbital per atom, the atom and electron indices are the same. These orbitals formally have sp^2-sp^3 hybridization. The nearest-neighbor hopping integral t_{ij} is parametrized/linearized as $t_{ij} = t_0 - \alpha(|\vec{r}_i - \vec{r}_j| - d_0)$, where t_0 is the average hopping integral, α is the electron-lattice interaction, and $\vec{r}$ is the carbon atom position. The second term in eq 2 is the lattice energy, which represents the effective nuclei-nuclei attraction and serves as the ionic background. All the parameters (t_0, α, K) are adjusted to match the experimental bond lengths of 1.4 and 1.46 Å and the energy gap of 2.0 eV between the LUMO and HOMO.

The total energy of the system can be expressed as

$$E(\{r\}) = \sum_{l}^{occ} \epsilon_l(\{r\}) + \frac{K}{2}\sum_{ij}(|\vec{r}_i - \vec{r}_j| - d_0)^2 \quad (3)$$

where the first term is the electron energy and the second term is the lattice energy. l is the energy level index. For the charge transfer process, we add an electron to energy level 31, so that the whole system has 61 electrons. We then compute the force by differentiating the energy with respect to the position of each atom. To simulate the photoexcitation,[105] we remove one electron from level 30 and put it into level 31. Our first finding is that charge transfer relaxation takes place on a time scale of 300−700 fs (see Figure 7).[91] The layer numbers in Figures 7 and 8 refer to the layers of equivalent bonds in Figure 2. The bond distortion is computed from the difference between the original and dynamical bond lengths. Therefore, at $t = 0$ fs, all of the bond distortion is zero (a straight horizontal line). At time 350 $\tau \approx 700$ fs ($\tau = 2.11$ fs is the integration step), two distinctive features are noted. First, the maximum deviation is in the center layer 7. The second maximum change is in the layers 6 and 8, but this is an opposite length change. Since the center layer has shorter bonds and the sixth and eighth ones have longer bonds, this opposite change effectively leads to a smaller difference between these two kinds of bonds. For other layers, the bond change within each layer is similar and will converge to the exact same place once the relaxation is completely over. Second, the distortions at the top and bottom layers are much smaller. This results in a typical polaron structure, where structurally the bond distortion is localized around the equator and electronically localized states appear in the HOMO−LUMO gap.

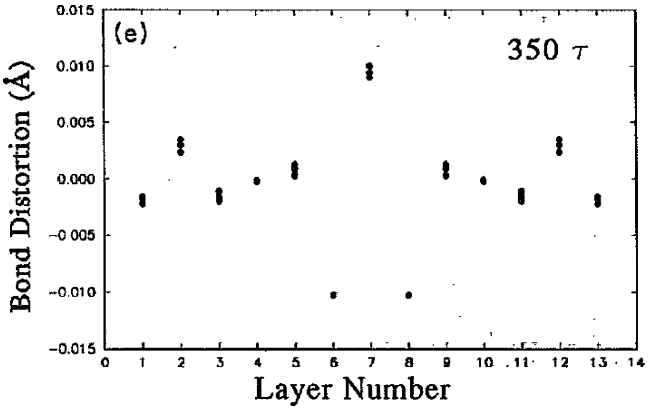

Figure 7. Relaxation of charge transfer, which needs 300 fs to finish. The configuration is shown at 700 fs ($\tau = 2.11$ fs is the integration step).[91] The layer number refers to those layers in Figure 2. The bond distortion is the difference between the current and original bond lengths.

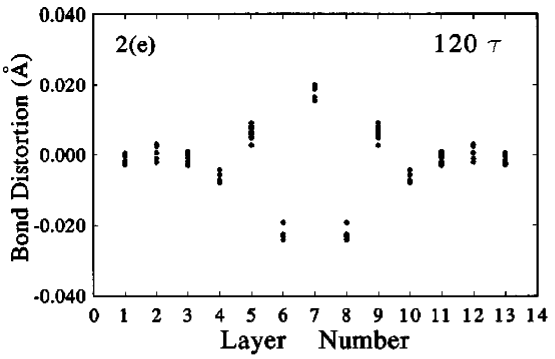

Figure 8. Relaxation of photoexcitation needs 100 fs to finish. The configuration shown is at 240 fs.[106]

The photoexcitation/relaxation finishes within 120−240 fs,[106] where Figure 8 shows the completed relaxation. This looks similar to the charge transfer case, but the bond change difference among different layers becomes smaller. In particular, layers 5 and 9 have a similar change as those in layers 6 and 8. Comparing with charge transfer, the photoexcitation proceeds much faster. This huge difference was first observed in polyacetylene.[104] The reason is that in charge transfer only one force from the additional electron is exerted on the lattice, but

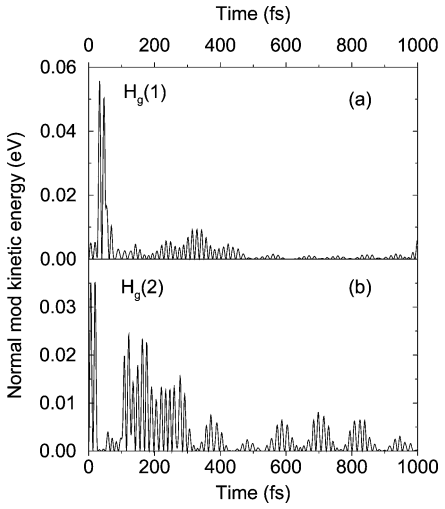

Figure 9. (a) Kinetic energy change of the $H_g(1)$ mode as a function of time. (b) Kinetic energy change of the $H_g(2)$ mode as a function of time.[108]

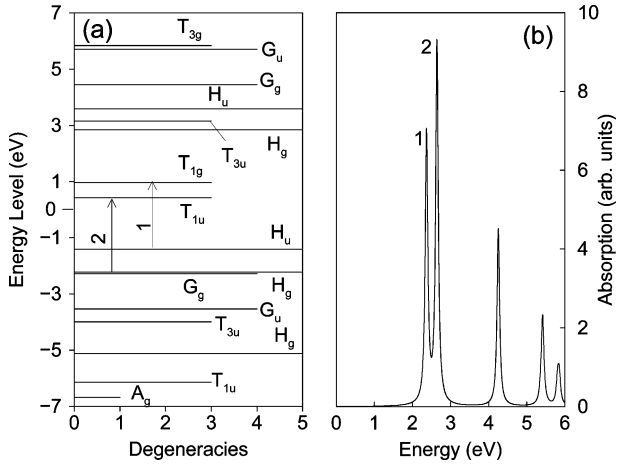

Figure 10. (a) Energy level scheme of C_{60}. (b) Absorption spectrum.[101]

in the photoexcitation, there are two forces, one from the electron in the LUMO and the other from the hole in the HOMO.

Using a similar formalism, Bruening and Friedman[107] simulated the charge transfer between a conducting polymer and C_{60} via a coupled Su-Schrieffer-Heeger model, and they found the photoinduced electron transfer taking place in 200−300 fs. They also considered the nonadiabatic process.

To investigate how the normal modes evolve with time, we introduce a kinetic-energy-based normal-mode analysis.[108] The idea is that instead of expanding the potential energy, we expand the kinetic energy in terms of normal modes as

$$K = \sum_{\mu} K_{\mu} = \frac{m}{2}\sum_{\mu} \dot{Q}_{\mu}^{2}; \quad \dot{Q}_{\mu} = \sum_{i} \mathbf{V}(i) \cdot \mathbf{G}_{\mu}(i) \qquad (4)$$

where $\mathbf{V}(i)$ and $\mathbf{G}_{\mu}(i)$ are the velocities of atom i and the normal mode eigenvector of mode μ, respectively. The reason is that the kinetic energy expansion is exact since the highest order of the kinetic energy is two, whereas the potential energy is not since high-anharmonic terms will appear. Figure 9 shows the kinetic energy changes in the $H_g(1)$ and $H_g(2)$ modes, both of which are Jahn-Teller active modes. One sees that the kinetic energy in the $H_g(2)$ mode relaxes more slowly than $H_g(1)$, and the major lattice energy is contained in the $H_g(1)$ mode, which has a lower frequency. These modes are mainly responsible for the superconductivity.

B. Laser-Induced Dynamics. When we include a laser field in our simulations, a time-dependent term must be added to the original Hamiltonian (eq 2). Starting now, we use the Hamiltonian of You et al.[109]

$$H_0 = -\sum_{ij,\sigma} t_{ij}(c_{i,\sigma}^{\dagger}c_{j,\sigma} + h.c.) + \frac{K_1}{2}\sum_{i,j}(r_{ij} - d_0)^2 + \frac{K_2}{2}\sum_{i} d\theta_{i,5}^{\ 2} + \frac{K_3}{2}\sum_{i}(d\theta_{i,6,1}^{\ 2} + d\theta_{i,6,2}^{\ 2}) \qquad (5)$$

including their parameters, since theirs fit not only the bond lengths and energy gap but also the normal-mode frequencies, and their lattice term contains bending and stretching modes (see the last two terms). Attached to each atom i are three bond angles: one is from an adjacent pentagon and two are from two hexagons. $\theta_{i,5}$ represents the bond angle around the pentagons, and its deviation from 108° is $d\theta_{i,5} = \theta_{i,5} - 108°$. $\theta_{i,6,1}$ and $\theta_{i,6,2}$ represent two bond angles around the hexagons, and their deviations from 120° are $d\theta_{i,6,1} = \theta_{i,6,1} - 120°$ and $d\theta_{i,6,2} = \theta_{i,6,2} - 120°$. You et al.[109] have determined the above parameters as $t_0 = 1.91$ eV, $\alpha = 5.0$ eV/Å, $K_1 = 42$ eV/Å^2, $K_2 = 8$ eV/rad^2, $K_3 = 7$ eV/rad^2 and $d_0 = 1.5532$ Å. Our laser field is represented by $H_I = -e\vec{F}(t)\cdot\sum_{i\sigma} n_{i\sigma}\vec{r}_i$. The laser envelope function is $\vec{F}(t)$, $n = c^{\dagger}c$, and e is the electron charge. If the laser field is a weak and continuous wave, we can use perturbation theory and Fourier transform the time-dependent problem to the frequency domain. As a result, the optical absorption can be computed from

$$\alpha(\hbar\omega) \propto \sum_{ij} \frac{|\langle i|\vec{D}|j\rangle|^2}{E_j - E_i - \hbar\omega + i\Gamma} \qquad (6)$$

where $\langle i|\vec{D}|j\rangle$ is the transition matrix element between states i and j, E_i is the eigenenergy (see Figure 10a), $\hbar\omega$ is the incident photon energy, and Γ is the damping. Figure 10b shows the absorption spectrum, where the numbers 1 and 2 represent two transitions highlighted in Figure 10a.

If the laser field is a Gaussian pulse and if the field strength is strong, we must go beyond perturbation theory and solve two coupled time-dependent equations for the electron and lattice. The electron dynamics is described by the Liouville equation

$$i\hbar\langle i|\dot{\rho}_{\sigma}|j\rangle = \langle i|[H, \rho_{\sigma}]|j\rangle \qquad (7)$$

where $H = H_0 + H_I$ and the density matrix is $\langle i|\rho_{\sigma}|j\rangle = \langle c_{i\sigma}^{\dagger}c_{j\sigma}\rangle$. Using the density matrix avoids dealing explicitly with multielectron wave functions and their orthogonalization. The density matrix formalism is also advantageous over the dark evolution method since it allows for fractional electron occupations and enables us to investigate the electron number change upon laser excitation. In eq 7, (i, j) may represent either a state or site index, but we find it is much easier to perform a calculation in position space for two reasons. First, the force along the x direction on the carbon atom i can be computed analytically as[108]

$$f_{i,x} = -\sum_{j(i)} 2\alpha\frac{\partial r_{ij}}{\partial x_i}\rho_{ij} - K\sum_{j(i)}(r_{ij} - d_0)\frac{\partial r_{ij}}{\partial x_i} \qquad (8)$$

where $j(i)$ refers to the summation taken over the nearest neighbor of site i. Forces along other directions can be computed analogously. Here we use the Hellmann−Feynman theorem to compute the force.[110] Second, since the state representation is constructed from a fixed atomic configuration, it is not as flexible

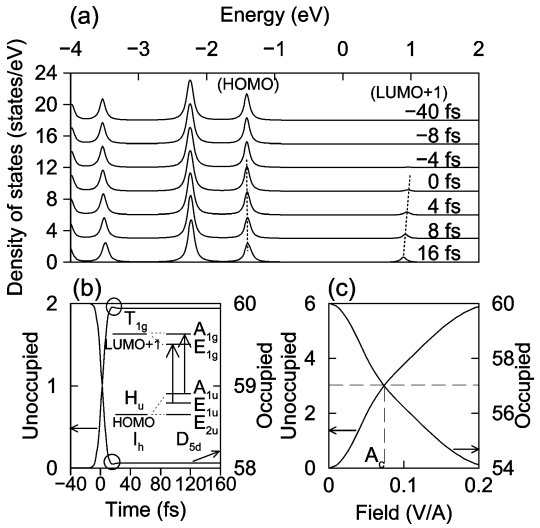

Figure 11. (a) Density of states versus energy as time progresses. The Fermi level is at 0 eV. The dotted line highlights the shift of the density of states due to the Jahn-Teller effect. (b) Electron number change in the occupied and unoccupied states as a function of time, where the two circles highlight "under/overshooting". The inset shows the energy level scheme. (c) Dependence of the number of excited electrons on the laser field amplitude.[101]

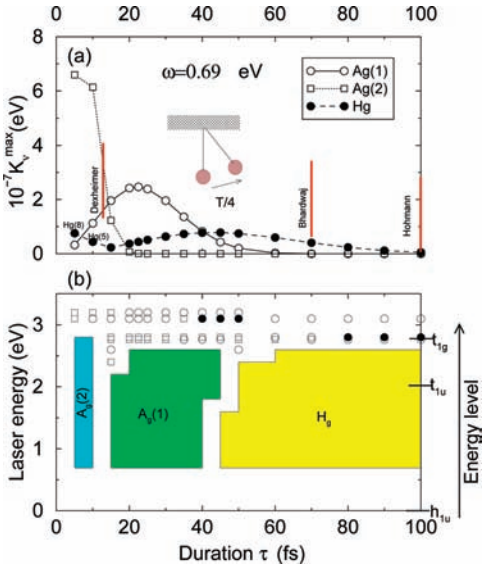

Figure 12. (a) Dependence of the maximal kinetic energy K_ν^{max} on the laser duration τ. The photon energy is $\omega = 0.69$ eV. (The results are similar for $\omega = 2.0$ eV.) The empty circles, boxes and filled circles denote the kinetic energies in the $A_g(1)$, $A_g(2)$, and H_g modes, respectively. Three experimental durations are denoted by three vertical bars (Dexheimer's duration[44] on the left, Bhardwaj's[96] in the center, and Hohmann's[85] on the right). Inset: model pendulum. (b) Laser-frequency versus pulse duration excitation diagram. The three shaded zones represent the excitation dominated by the $A_g(2)$, $A_g(1)$, and H_g modes. The empty circles, boxes and filled circles have the same meanings as those in (a). The labels on the right vertical axis indicate the electronic energy levels of C_{60}.[113]

as the site representation. In other words, the state space is not large enough to describe the change in phase space.

The energy level scheme and absorption spectrum of C_{60} (see Figure 10) serve as a good guide to excite a specific state. Figure 11a shows the change in density of states as a function of time. Here we use a Gaussian pulse of duration of 10 fs and laser energy of 2.37 eV (exactly at the first absorption peak). The electron excitation is very quick, and within 16 fs, the final density of states is nearly formed. Since the first dipole-allowed transition is between HOMO and LUMO+1, the density accumulates mainly at LUMO+1. These changes can be directly probed experimentally.[51,100] As time evolves, the LUMO+1 and HOMO states move closer to the Fermi level (0 eV). This change is a result of lattice relaxation, similar to what we have found in the dark evolution. The energy level change is schematically shown in the inset of Figure 11b, where the symmetry is reduced from I_h to D_{5d}. The detailed electron number change is shown in Figure 11b. We see that the major electron number change occurs within 20 fs. There is an "under/overshooting" (see the two circles) before the electron occupations finally settle down to their final results, which is consistent with the experimental observations.[111] The field dependence is plotted in Figure 11c. One sees a superlinear increase at first, and after a critical field strength of $A_c = 0.07$ V/Å, it starts to saturate.

C. Laser Pulse Duration Control of Vibrational Mode Excitation. Experimental investigations have revealed enormous insight into the ultrafast dynamics in C_{60}, but there has been a long-standing puzzle as to why some experiments only reveal A_g modes, while others reveal H_g modes. For example, Dexheimer et al.[44] showed that only two A_g modes were excited in their spectrum, while Hohmann et al.,[85] Bhardwaj et al.,[96] Boyle et al.,[112] and Laarmann et al.[100] detected only the H_g modes. We note that these normal mode excitations are all formally allowed by the selection rules. The Jahn−Teller active modes are the H_g modes, but in laser excitation the A_g modes are excitable as well.

With the great success in simulating and understanding both electron and lattice dynamics, we are ready to resolve this long-time controversy. These earlier experiments used very different wavelengths, intensities and pulse durations, which requires an extensive theoretical investigation. Our study begins with the above standard Hamiltonian, eq 5, where all of the parameters are fixed. In the meantime, all of the laser parameters are determined experimentally. This essentially leaves us no adjustable parameters to match the experimental results, a very critical test for our theoretical model. As described above, we also use the normal mode kinetic energy-based formalism to measure whether one particular mode is excited or not. Figure 12 shows a comprehensive excitation diagram, where the laser energy is 0.69 eV (the results are similar for the energy of 2.0 eV).[113] We note that only the dominant normal modes are included. Figure 12a shows the normal mode kinetic energy as a function of the laser pulse duration. One notices immediately that different normal modes dominate in different regions. For the shortest pulses, the high-energy modes $A_g(2)$ and $H_g(8)$ dominate, followed by the $A_g(1)$ mode. When the laser pulse duration prolongs to 12 fs (which is Dexheimer's pulse duration), we see the $A_g(1)$ and $A_g(2)$ modes dominate, and H_g drops sharply. This result is fully consistent with the experimental results. We use vertical bars to highlight three experimental results. If we further increase our pulse duration to Bhardwaj's and Hohmann's pulse durations, we find now the H_g modes dominate. This explains the controversy among the different experiments; that is, the reason is that different pulse durations were used in these experimental investigations. We find the optimal condition for the dominance of these modes is that, for all of the nonresonant excitations, the ratio of the normal mode's period to laser pulse duration is about 3.4, a result that can be understood from a simple pendulum [see the inset in Figure 12a], where the optimal ratio is 4. Since the lattice does not couple to the laser field directly, there is a small mismatch. Figure 12b shows the laser energy dependence. The energy level

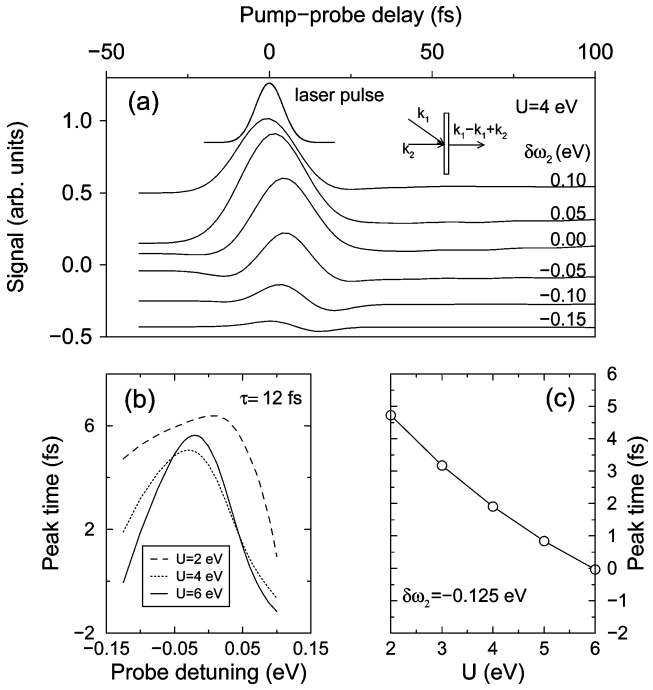

Figure 13. (a) Pump-probe signal as a function of the time delay between the pump and probe pulses for the probe detuning from $\delta\omega_2 = -0.15$ to $+0.10$ eV. The pump energy is 0.1 eV below E_0. A schematic of the pump-probe experimental transmission geometry is shown in the upper right inset. Although the pump pulse also transmits through the sample (vertical bar), only the signal along the direction $\vec{k}_1 - \vec{k}_1 + \vec{k}_2$ is probed. The pulse duration for both the probe and pump pulses is 12 fs. $A_1 = 0.05$ V/Å and $A_2 = 0.01$ V/Å. All of the curves are vertically shifted for a better view. (b) Peak time as a function of the probe detuning for $U = 2$ eV (dashed line), $U = 4$ eV (dotted line), and $U = 6$ eV (solid line). (c) Peak time as a function of U at probe detuning $\delta\omega_2 = -0.125$ eV.[116]

scheme is shown on the right-hand side. It is clear that when the energy is below 2 eV (the gap between the HOMO and LUMO), the excitation pattern is similar: $A_g(2)$ dominates from 5 to 10 fs pulse durations, $A_g(1)$ from 15 to 40 fs, and above 40 fs, H_g takes over. As a result, to investigate the superconductivity in alkali-doped C_{60}, the ideal pulse duration is about 60 to 80 fs. When the laser energy becomes close to the resonance energy (corresponding the first dipole-allowed transition of 2.75 eV), the excitation map changes dramatically. For instance, long pulses may also excite A_g modes. This excitation map is very useful experimentally in controlling a few normal mode excitations.

We have also investigated the laser intensity effect. We find that for a stronger laser, two A_g modes dominate. This finding is consistent with Torralva et al.'s results[114] who included the laser field in their simulations. They found the pentagonal-pinch mode is dominant at low fluence, and the breathing mode is dominant at high fluence.

D. Electron Correlation Effect Probed by Time-Dependent Pump−Probe Spectroscopy. Once we successfully include the laser field, we are ready to simulate a time-resolved pump−probe experiment. The experiment typically uses two laser pulses, where one is the pump and the other is the probe. The pump pulse first excites the system, and after a time delay, the probe pulse probes the dynamics left behind by the pump pulse. If we assign the wavevector $\vec{k}_1$ to the pump pulse and $\vec{k}_2$ the probe pulse, the signal propagating along $\vec{k}_1 - \vec{k}_1 + \vec{k}_2$ is detected experimentally [see the inset in Figure 13a]. By analyzing this signal as a function of time delay between pump and probe, one can learn the intrinsic properties of the system. Despite the simple experimental geometry, there are two theoretical complications. First, the signal is probed at the far field, while all the interactions and dynamics occur in the near field. One has to find a way to compute the far-field signal from the near-field response. Theoretically, if the system is large enough, one can perform the Fourier transform to momentum space, and then keep those Fourier coefficients for the far-field calculation. However, since in C_{60} the dimension is so small, the product of the position and light wavevector k is very small or close to zero, and nearly all the components in this region have a similar value. Second, only one component is probed experimentally, but the density matrix in the Liouville equation (7) contains all the orders and has contributions from all the directions. To make a comparison with the experiment, one has to sort out these contributions.

A common scheme to overcome these difficulties is the rotating-wave approximation.[115] It is known that any far-field signal propagates with a phase factor of $\exp(-i(\vec{k}\cdot\vec{r} - \omega t))$, where $\vec{k} = n\vec{k}_1 + m\vec{k}_2$, $\omega = n\omega_1 + m\omega_2$, and n and m are the orders in the pump and probe fields. Although we can not use $\vec{k}\cdot\vec{r}$ to distinguish the directions since the value is too small, we can use the frequency factor $e^{i\omega t}$ to label those density matrices along different directions.[101] In other words, the density matrix ρ becomes ρ_ω or ρ_k. This is achieved by first expanding the laser fields and then the density matrix. The pump pulse is

$$F_p = (E_p^* e^{i(\vec{k}_1\cdot\vec{r}-\omega_1 t)} + E_p e^{-i(\vec{k}_1\cdot\vec{r}-\omega_1 t)})/2 \tag{9}$$

and the density matrix becomes

$$\rho = \sum_{nm} \rho^{(n|m)} e^{i(n\vec{k}_1 + m\vec{k}_2)\cdot\vec{r} - i(n\omega_1 + m\omega_2)t} \tag{10}$$

where $\rho^{(n|m)}$ represents that element of the matrix which interacts with the pump field n times and probe m times. This is just ρ_ω or ρ_k. If there are three laser pulses, the density matrices will have three indices. Terms like $E_p\rho$ become

$$\rho E_p = \frac{1}{2}\sum_{nm} (\rho^{(n-1|m)} E_p^* + \rho^{(n+1|m)} E_p) e^{i(n\vec{k}_1 + m\vec{k}_2)\cdot\vec{r} - i(n\omega_1 + m\omega_2)t} \tag{11}$$

Then, we perform a similar calculation for the remaining terms in the above Liouville equation, eq 7, and equate the coefficients of $e^{i(n\vec{k}_1 + m\vec{k}_2)\cdot\vec{r}}$ on both sides, which leads to[116]

$$\begin{aligned} i\hbar\dot{\rho}_{ij}^{(n|m)} = &-\hbar(n\omega_1 + m\omega_2)\rho_{ij}^{(n|m)} + \sum_l (t_{il}\rho_{lj}^{(n|m)} - \rho_{il}^{(n|m)} t_{lj}) + \\ &\vec{F}_1 \cdot (\vec{r}_i - \vec{r}_j)\rho_{ij}^{(n-1|m)} + \vec{F}_1^* \cdot (\vec{r}_i - \vec{r}_j)\rho_{ij}^{(n+1|m)} + \\ &\vec{F}_2 \cdot (\vec{r}_i - \vec{r}_j)\rho_{ij}^{(n|m-1)} + \vec{F}_2^* \cdot (\vec{r}_i - \vec{r}_j)\rho_{ij}^{(n|m+1)} + \\ &U\sum_{\alpha,\beta} [\rho_{ii}^{(n-\alpha|m-\beta)} - \rho_{jj}^{(n-\alpha|m-\beta)}]\rho_{ij}^{(\alpha|\beta)} \end{aligned} \tag{12}$$

Here ω_1 and ω_2 are the frequencies of the pump and probe pulses, U is the on-site interaction,[117] and F_1 and F_2 are their respective field strengths. The element $\rho^{(n|m)}$ is used to compute experimentally observed signals. If we are interested in a pump-probe signal, we choose $\rho^{(1-1|1)}$ to compute the signal.

Figure 13a shows the pump-probe signal as a function of time delay between the pump and probe pulses as the probe detuning increases from bottom to top. This detuning is referenced with respect to the first dipole-allowed transition at 2.75 eV between the HOMO and LUMO+1. It is clear that the signal peaks around 0 fs. However, its peak time changes with the photon

energy, as expected. Figure 13b shows the details of the peak shift for different on-site interactions U. As U increases, the peak becomes sharper. The on-site interaction also directly pushes the peak time to an earlier time scale (Figure 13c), since a larger on-site repulsion leads to an immediate suppression of the excitation of the electron dynamics. This feature should be useful for estimating the strength of the electron correlation for future experimental investigations.

E. High-Order Harmonic Generation. Although experimental investigations of harmonic generation in C_{60} started early on, the current harmonic order is limited to the fifth order. In 2001, Bauer et al. numerically investigated the possibilities to generate even higher harmonic generation under the influence of intense femtosecond laser pulses.[118]

The advantage of using C_{60} as a medium is apparent since it has a large cross section, leading to a larger signal than that in atoms, provided the laser intensity is below the fragmentation threshold. We have explored high-harmonic generation in C_{60} using our tight-binding model Hamiltonian. The whole calculation is not very different from the above, but the emission spectrum is directly computed from the dipole acceleration operator. This is the term that normally is on the right-hand side of Maxwell's equation as the source of the radiation. To be more specific, the expression of the dipole acceleration is[119]

$$\ddot{d}(\Omega) = \sqrt{(\ddot{d}_x(\Omega))^2 + (\ddot{d}_y(\Omega))^2 + (\ddot{d}_z(\Omega))^2} \qquad (13)$$

where $\ddot{d}_x(\Omega)$, $\ddot{d}_y(\Omega)$, and $\ddot{d}_z(\Omega)$ are the Fourier components along the x, y, and $z$directions, respectively. The laser polarization can be linear, circular, or elliptical. For the linear polarization, the result is the same for different directions due to the nearly spherical symmetry of C_{60}. Figure 14 shows a typical high-harmonic generation in C_{60}. Here the laser energy is 0.4 eV and field strength is 0.02 V/Å. The pulse shape is sine-squared with duration of $\tau = 32$ laser field cycles. Figure 14a shows that below the seventh order, the harmonic generation is quite normal in the sense that all the peaks appear at odd numbers, such as peaks b, c and d. Peak a comes from the vibrations of the atoms. For the harmonics higher than the seventh order, they appear rather random. In order to understand these features, Figure 14b shows how the emitted energy depends on the incident laser energy. One notices that for the first- and third-order harmonics there is a linear dependence, but for the harmonic peak e (in Figure 14), it does not change with the incident energy. This is proof that those high-order peaks result from internal transitions in C_{60}. Figure 14c shows that all of those high-order harmonics correspond to the allowed transitions.

The harmonic yield also depends on the laser polarization. For an elliptically circularly polarized light, the yield shows a dramatic change as we change the polarization.[120] Figure 15a shows for the ordinary harmonics there is a monotonic decrease with the laser ellipticity. The dependence is independent of laser intensity. For instance, if the intensity is increased twice, the dependence stays the same (see Figure 15a). But for those harmonics resulting from the internal transitions, their low- and high-intensity behaviors differ substantially (see Figure 15b). For the high intensity, an anomaly can be observed clearly, where the harmonic yield maxima appear at a nonzero ellipticity. The reason for such an anomaly is a result of the competition between the earlier saturation at zero ellipticity and the slower saturation at nonzero ellipticity. We conclude such a anomaly only occurs at a high-intensity limit. We expect that future experiments can directly check our predictions.

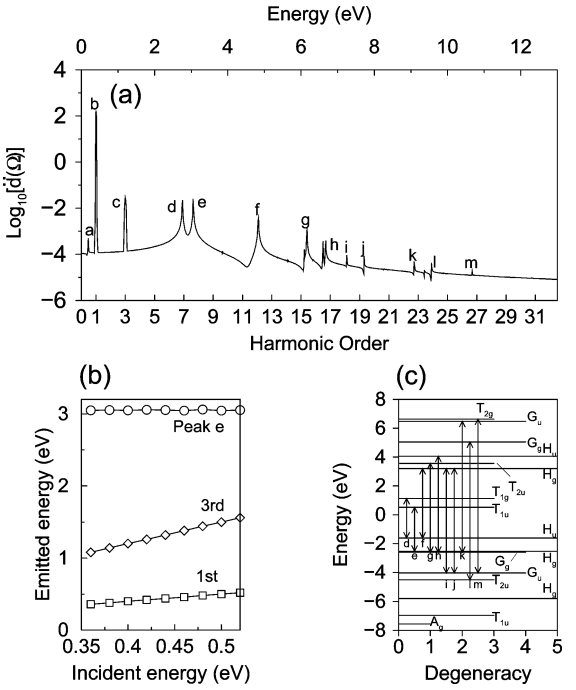

Figure 14. (a) Harmonic generations in C_{60}. The laser energy is 0.4 eV, pulse duration is 32 laser cycles, and field strength is 0.02 V/Å. Peak a results from the lattice vibration. Peaks b, c, and d are at the first, third and seventh orders, respectively. Above the seventh order, harmonics mainly result from the intrinsic electronic excitations. (b) Emitted photon energy versus the incident energy. The circles, diamonds and squares denote peak e, the third and first harmonics, respectively. (c) Assignment of peaks from d to m (see letters below arrows) to their respective transitions (double-arrowed lines). H_u (HOMO) is at -1.6158 eV, and T_{1u} (LUMO) is at 0.5255 eV.[119]

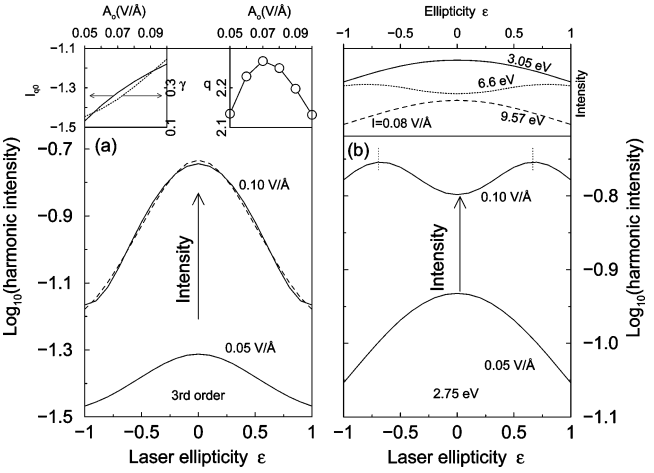

Figure 15. (a) Ellipticity dependence of the third-harmonic generation. The incident laser intensity increases from 0.05 to 0.10 V/Å. (b) Ellipticity dependence of the harmonic generation at 2.75 eV. This harmonic corresponds to the transition between HOMO and LUMO+1. An increase in the laser intensity splits the peak into two and moves the maximal harmonic intensity to $\epsilon = 0.7$. The vertical dashed lines highlight the peak change. Inset: Dependence on the incident light ellipticity for higher harmonics, where the laser intensity is 0.08 V/Å. All of the curves are vertically shifted for clarity.[120]

V. Prospectives and Possible Applications

Intensive studies of ultrafast dynamics in C_{60} over the past decade have paved the way to future investigations and possible applications. Here, we present our own prospectives by introducing several new important discoveries.

Superconductivity. On the fundamental side of science, Brorson et al.[121] and Fleischer et al.[122] reported investigations of femtosecond optical dynamics in alkali-doped C_{60} superconductor. This study represents a major step toward understanding superconductivity on the time scale in C_{60}. They found a fast response of 200 fs in both Rb_3C_{60} and K_3C_{60} as compared with the undoped C_{60}. The differential reflectance change appears featureless, but with some very small oscillations. Maybe due to the relatively long pulse (50 fs), neither C_{60} nor alkali-doped C_{60} show the clear phonon oscillation as seen by Dexheimer et al.,[44] but when they used a 10 fs Ti:sapphire laser, they surely observed the strong oscillation of the $A_g(1)$ mode.[123] Its oscillation has a long life of over 2 ps. No effort was made to extract $A_g(2)$ and H_g modes from their spectra, which may contain crucial information about the relaxation of H_g modes and connection to superconductivity. Their latter work used a longer pulse (120−200 fs),[124] which may potentially blur some crucial signature of the participation of H_g phonon modes, which is at the core of the superconductivity. Future experiments must use a short and variable pulse duration to scan across different regions to selectively excite the phonon modes, since they hold the key to a complete understanding of the superconductivity. It is important to go beyond a mechanism based on a thermal activation process.[125] This may serve as a useful case study of ultrafast dynamics in high-temperature superconductors.[126]

Control of Normal Mode Excitation. Another largely unexplored field is vibrational mode control in C_{60}.[127] It is almost routine to map out the vibrational modes systematically in small molecules, but in a big molecule like C_{60}, this is still very challenging. However, the benefit is enormous since C_{60} will share many features of a large system, and any knowledge gained from the ultrafast dynamics in C_{60} will be very useful to control and manipulate the dynamics in even much larger systems.

Second-Harmonic Generation (SHG). In 1996, Kuhnke et al.[128] found that the SHG from the single-crystal C_{60} surface can be partially switched off by a second pump pulse on the exit surface of the SHG.[129] Different from several earlier samples, since their sample is a single crystal, this allows them to map out the polarization dependence at different angles, a study which has a profound impact on future research. The signal drops to 35% of the original SHG. This is a very interesting result, and it may indicate a possible ultrafast switching gate, where a weak beam can sufficiently control the SHG yield. However, various laser intensities were used in their experiments, which makes a quantitative understanding difficult.

Light-Emitting Device (LED). Another important field is the fullerene-based LED, which has been reviewed recently.[30] At the center is the large π-electron delocalization, which renders a very fast response to ultrafast laser excitation. These excellent nonlinear optical properties are promising for LEDs, a process involving charge transfer and light excitation. In particular, a possible solar energy converter is of great interest.[130] In 2007, Lioudakis et al.[131]investigated exciton intraband relaxation and electron/polaron relaxation of dissociated excitons in PCBM for different concentrations. They observed the intraband relaxation constant of 0.5−1.5 ps. The second long-lived relaxation of 0.5−1 ns is assigned to the fullerene. In 2008, Hwang et al.[132] showed that mobile carriers in regioregular poly(3-hexylthiophene) and the [6,6]-phenyl-C_{61} butyric acid methyl ester fullerene derivative are generated via a two-step process: initial ultrafast charge separation to an intermediate charge transfer bound state, followed by the transfer of carriers onto the bicontinuous networks, similar to the above. By annealing bulk heterojunction blends, they reduced the recombination loss of mobile carriers by a factor of 2.5, which is very promising.

Acknowledgment. This work was supported by the U.S. Department of Energy under Contract No. DE-FG02-06ER46304, the U.S. Army Research Office under Contract W911NF-04-1-0383, and a Promising Scholars grant from Indiana State University. In addition, we acknowledge part of the work done on Indiana State University's high-performance computers. This research used resources of the National Energy Research Scientific Computing Center, which is supported by the Office of Science of the U.S. Department of Energy under Contract No. DE-AC02-05CH11231. This project was also supported by the National Natural Science Foundation of China under Grant No. 20674010.

References and Notes

(1) Etemad, S.; Fann, W-S.; Townsend, P. D.; Baker, G. L.; Jackel, J. In *Conjugated Polymeric Materials: Opportunities in Electronics, Optoelectronics and Molecular Electronics*; Bredas, J. L., Chance, R. R., Eds.; NATO ASI Ser. E; Kluwer: Dordrecht, The Netherlands, 1990; p 341, Vol. 182.
(2) Feject, M. M. *Phys. Today* **1994**, *47* (5), 25.
(3) Garmire, E. *Phys. Today* **1994**, *47* (5), 42.
(4) Garito, A.; Shi, R. F.; Wu, M. *Phys. Today* **1994**, *47* (5), 51.
(5) Zhang, G. P.; George, T. F.; Pandey, L. N. *J. Chem. Phys.* **1998**, *109*, 2562.
(6) Zhang, G. P. *Phys. Rev. B* **1999**, *60*, 11482.
(7) Xu, M.; Sun, X. *Phys. Rev. B* **2000**, *61*, 15766.
(8) Zhang, G. P. *Phys. Rev. B* **2000**, *61*, 4377.
(9) Zhang, G. P.; George, T. F. *Phys. Rev. B* **2001**, *63*, 113107.
(10) Champagne, B.; Spassova, M.; Jadin, J.-B.; Kirtman, B. *J. Chem. Phys.* **2002**, *116*, 3935.
(11) Zhang, G. P. *Phys. Rev. Lett.* **2001**, *86*, 2086.
(12) Shakin, V. A.; Abe, S. *Phys. Rev. B* **1994**, *50*, 4306.
(13) Islam, M. N. *Phys. Today* **1994**, *47* (5), 34.
(14) Marder, S. R.; Perry, J. W.; Schaefer, W. P. *Science* **1989**, *245*, 626. Marder, S. R.; Beratan, D. N.; Cheng, L.-T. *Science* **1991**, *252*, 103. Marder, S. R.; Perry, J. W.; Bourhill, G.; Gorman, C. B.; Tiemann, B. G.; Mansour, K. *Science* **1993**, *261*, 186.
(15) Marder, S. R.; Cheng, L.-T.; Tiemann, B. G.; Friedli, A. C.; Blanchard-Desce, M.; Perry, J. W.; Skindhj, J. *Science* **1994**, *263*, 511.
(16) Cumpston, B. H.; Ananthavel, S. P.; Barlow, S.; Dyer, D. L.; Ehrlich, J. E.; Erskine, L. L.; Heikal, A. A.; Kuebler, S. M.; Lee, I.-Y. S.; McCord-Maughon, D.; Qin, J.; Rckel, H.; Rumi, M.; Wu, X.-L.; Marder, S. R.; Perry, J. W *Nature* **1999**, *398*, 51.
(17) Shen, Y. R. *The Principles of Nonlinear Optics*; Wiley: New York, 2003. Boyd, R. W. *Nonlinear Optics*; Academic Press: San Diego, 1992. (c) Mukamel, S. *Principles of Nonlinear Optics and Spectroscopy*; Oxford University Press: Oxford, 1995.
(18) Kroto, H. W.; Heath, J. R.; O'Brien, S. C.; Curl, R. F.; Smalley, R. E. *Nature* **1985**, *318*, 162.
(19) Blau, W. J.; Byrne, H. J.; Cardin, D. J.; Dennis, T. J.; Hare, J. P.; Kroto, H. W.; Taylor, R.; Walton, D. R. M. *Phys. Rev. Lett.* **1991**, *67*, 1423.
(20) Kafafi, Z. H.; Bartoli, F. J.; Lindle, J. R.; Pong, R. G. *Phys. Rev. Lett.* **1992**, *68*, 2705.
(21) Kafafi, Z. H.; Lindle, J. R.; Pong, R. G. S.; Bartoli, F. J.; Lingg, L. J.; Milliken, J. *Chem. Phys. Lett.* **1992**, *188*, 492.
(22) Knize, R. J.; Partanen, J. P. *Phys. Rev. Lett.* **1992**, *68*, 2704.
(23) Hoshi, H.; Nakamura, N.; Maruyama, Y.; Nakagawa, T.; Suzuki, S.; Shiromaru, H.; Achiba, Y. *Jpn. J. Appl. Phys.* **1991**, *30*, L1397.
(24) Tutt, L. W.; Kost, A. *Nature* **1992**, *356*, 225.
(25) Allaf, A. W.; Zidan, M. D. *Opt. Lasers Eng.* **2005**, *43*, 57.
(26) Elim, H. I.; Ji, W.; Meng, G. C. *J. Nonlinear Opt. Phys. Mater.* **2003**, *12*, 175.
(27) McLean, D. G.; Sutherland, R. L.; Brant, M. C.; Brandelik, D. M.; Fleitz, P. A.; Pottenger, T. *Opt. Lett.* **1993**, *18*, 858.
(28) Liu, H.; Taheri, B.; Jia, W. *Phys. Rev. B* **1994**, *49*, 10166.
(29) Huo, Y. P.; Zeng, H. P.; Jiang, H. F. *Chin. J. Org. Chem.* **2004**, *24*, 1191.
(30) Martin, N.; Sanchez, L.; Herranz, M. A.; Illescas, B.; Guldi, D. M. *Acc. Chem. Res.* **2007**, *40*, 1015.
(31) Rustagi, K. C.; Nair, S. V.; Ramaniah, L. M. *Prog. Cryst. Growth Charact. Mater.* **1997**, *34*, 81.
(32) Belousov, V. P.; Belousova, I. M.; Budtov, V. P.; Danilov, V. V.; Danilov, O. B.; Kalintsev, A. G.; Mak, A. A. *J. Opt. Technol.* **1997**, *64*, 1081.

(33) Shinar, J.; Vardeny, Z. V.; Kafafi, Z. H. *Optical and Electronic Properties of Fullerenes and Fullerene-Based Materials*; Marcel Dekker: New York, 2000.
(34) Gong, Q. H.; Sun, Y. X.; Xia, Z. J.; Zou, Y. H.; Gu, Z. N.; Zhou, X. H.; Qiang, D. *J. App. Phys.* **1992**, *71*, 3025. Tang, N.; Partanen, J. P.; Hellwarth, R. W.; Knize, R. J. *Phys. Rev. B* **1993**, *48*, 8404.
(35) Lindle, J. R.; Pong, R. G. S.; Bartoli, F. J.; Kafafi, Z. H. *Phys. Rev. B* **1993**, *48*, 9447.
(36) Strohkendl, F. P.; Axenson, T. J.; Larsen, R. J.; Dalton, L. R.; Hellwarth, R. W.; Kafafi, Z. H. *J. Phys. Chem. B* **1997**, *101*, 8802. Strohkendl, F. P.; Larsen, R. J.; Dalton, L. R.; Kafafi, Z. K. *Chem. Phys. Lett.* **2000**, *331*, 354.
(37) Neher, D.; Stegeman, G. I.; Tinker, F. A.; Peyghambarian, N. *Opt. Lett.* **1992**, *17*, 1491.
(38) Meth, J. S.; Vanherzeele, H.; Wang, Y. *Chem. Phys. Lett.* **1992**, *197*, 26.
(39) Kajzar, F.; Taliani, C.; Danieli Rossini, R. S.; Zamboni, R. *Chem. Phys. Lett.* **1994**, *217*, 418.
(40) Banfi, G.; Fortusini, D.; Bellini, M.; Milani, P. *Phys. Rev. B* **1997**, *56*, R10075.
(41) Bezel, I. V.; Chekalin, S. V.; Matveets,Yu, A.; Stepanov, A. G.; Yartsev, A. P.; Letokhov, V. S. *Chem. Phys. Lett.* **1994**, *218*, 475.
(42) Yamaguchi, S.; Tahara, T. *Chem. Phys. Lett.* **2004**, *390*, 136.
(43) Talapatra, G. B.; Manickam, N.; Samoc, M.; Orczyk, M. E.; Karna, S. P.; Prasad, P. N. *J. Phys. Chem.* **1992**, *96*, 5206.
(44) Dexheimer, S. L.; Mittleman, D. M.; Schoenlein, R. W.; Vareka, W.; Xiang, X.-D.; Zettl, A.; Shank, C. V. In *Ultrafast Phenomena VIII*; Springer Series in Chemical Physics; Martin, J.-L., Migus, A., Mourou, G. A., Zewail, A. H., Eds.; Springer-Verlag: Berlin, 1993; p 81, Vol. 55.
(45) Bendikov, M.; Wudl, F.; Perepichka, D. F. *Chem. Rev.* **2004**, *104*, 4891.
(46) Xenogiannopoulou, E.; Medved, M.; Iliopoulos, K.; Bonifazi, D.; Sooambar, C.; Mateo-Alonso, A.; Prato, M. *ChemPhysChem* **2007**, *8*, 1056.
(47) Mateo-Alonso, A.; Iliopoulos, K.; Couris, S.; Prato, M. *J. Am. Chem. Soc.* **2008**, *130*, 1534.
(48) Liu, Z.; Tian, J.; Zang, W.; Zhou, W.; Zhang, C.; Zheng, J.; Zhou, Y.; Xu, H. *Appl. Opt.* **2003**, *42*, 7072.
(49) Ganeev, R. A.; Ryasnyansky, A. I.; Kamanina, N. V.; Kulagin, I. A.; Kodirov, M. K.; Usmanov, T. *J. Opt. B* **2001**, *3*, 88.
(50) Qian, S. X.; Ma, G. H.; Chen, Y.; Cai, R. F.; Qian, W.; Lin, L.; Zou, Y. H. *J. Phys. Chem. Solids* **2000**, *61*, 1069.
(51) Hertel, I. V.; Laarmann, T.; Schulz, C. P. *Adv. At. Mol. Opt. Phys.* **2005**, *50*, 219. Schulz, C. P.; Burnus, T.; Castro, A.; Gross, E. K. U.; Heidenreich, A.; Hertel, I. V.; Jortner, J.; Laarmann, I.; Last, I.; Levis, R. J.; Marques, M. A. L.; Romanov, D. A.; Saenz, A. In *Analysis and Control of Ultrafast Photoinduced Reactions*; Köhn, O; Wöste, L., Eds.; Springer: Berlin, 2007; p 485.
(52) Andreoni, W. *Annu. Rev. Phys. Chem.* **1998**, *49*, 405. Huffman, D. R. *Phys. Today* **1991**, *44* (11), 22. Haddon, R. C. *Acc. Chem. Res.* **1992**, *25*, 127.
(53) Pickett, W. E. *Solid State Phys.* **1994**, *48*, 225. Dresselhaus, M. S.; Dresselhaus, G.; Eklund, P. C. *Science of Fullerenes and Carbon Nanotubes*; Academic Press: San Diego, 1996. Special issue on Buckminsterfullerenes *Acc. Chem. Res. March* **1992**, *25*(3).
(54) Rosker, M. J.; Marcy, H. O.; Chang, T. Y.; Khoury, J. T.; Hansen, K.; Whetten, R. L. *Chem. Phys. Lett.* **1992**, *196*, 427. Flom, S. R.; Pong, R. G. S.; Bartoli, F. J.; Kafafi, Z. H. *Phys. Rev. B* **1992**, *46*, 15598. Yung, M. F.; Wong, K. Y. *Appl. Phys. B: Laser Opt.* **1998**, *66*, 585.
(55) Drenser, K. A.; Larsen, R. J.; Strohkendl, F. P.; Dalton, L. R. *J. Phys. Chem. A* **1999**, *103*, 2290.
(56) Shuai, Z.; Bredas, J. L. *Phys. Rev. B* **1992**, *46*, 16135.
(57) Quong, A. A.; Pederson, M. R. *Phys. Rev. B* **1992**, *46*, 12906.
(58) Matsuzawat, N.; Dixon, D. A. *J. Phys. Chem.* **1992**, *96*, 6872.
(59) Takahashi, A.; Wang, H. X.; Mukamel, S. *Chem. Phys. Lett.* **1993**, *216*, 394.
(60) Li, J.; Feng, J. K.; Sun, J. Z. *Chem. Phys. Lett.* **1993**, *203*, 560.
(61) Westin, E.; Rosén, A. *Z. Phys. D* **1993**, *26*, 273. Westin, E.; Rosén, A. *Appl. Phys. A: Mater. Sci. Process.* **1995**, *60*, 49.
(62) Harigaya, K.; Abe, S *Jpn. J. Appl. Phys.* **1992**, *31*, L887.
(63) Hara, T.; Nomura, Y.; Narita, S.; Shibuya, T. *Chem. Phys. Lett.* **1995**, *240*, 610.
(64) Fanti, M.; Orlandi, G.; Zerbetto, F. *J. Am. Chem. Soc.* **1995**, *117*, 6101.
(65) Bechstedt, F.; Fiedler, M.; Sham, L. J. *Phys. Rev. B* **1999**, *59*, 1857.
(66) van Gisbergen, S. J. A.; Snijders, J. G.; Baerends, E. J. *Phys. Rev. Lett.* **1997**, *78*, 3097.
(67) Nomura, Y.; Miyamoto, T.; Hara, T.; Narita, S.; Shibuya, T. *J. Chem. Phys.* **2000**, *112*, 6603.
(68) Iwata, J.-I.; Yabana, K.; Bertsch, G. F. *J. Chem. Phys.* **2001**, *115*, 8773.
(69) Norman, P.; Luo, Y.; Jonsson, D.; Ågren, H. *J. Chem. Phys.* **1997**, *106*, 8788.
(70) Tsolakidis, A.; Sanchez-Portal, D.; Martin, R. M. *Phys. Rev. B* **2002**, *66*, 235416.
(71) Zhou, X.; Ren, A. M.; Feng, J. K. *J. Mol. Struct.* **2004**, *680*, 237.
(72) Jensen, L.; van Duijnen, P. Th. *Int. J. Quantum Chem.* **2005**, *102*, 612.
(73) Cheng, W.-D.; Wu, D.-S.; Zhang, H.; Chen, D.-G.; Wang, H. X. *Phys. Rev. B* **2002**, *66*, 113401.
(74) Martini, I. B.; Ma, B.; Da Ros, T.; Helgeson, R.; Wudl, F.; Schwartz, B. J. *Chem. Phys. Lett.* **2000**, *327*, 253.
(75) Mittal, J. P. *Pure Appl. Chem.* **1995**, *67*, 103.
(76) Sariciftci, N. S.; Heeger, A. J. *Int. J. Mod. Phys. B* **1994**, *8*, 237.
(77) Mihailetchi, V. D.; Koster, L. J. A.; Hummelen, J. C.; Blom, P. W. M. *Phys. Rev. Lett.* **2004**, *93*, 216601.
(78) Hwang, I. W.; Xu, Q. H.; Soci, C.; Chen, B. Q.; Jen, A. K. Y.; Moses, D.; Heeger, A. J *Adv. Funct. Mater.* **2007**, *17*, 563. Hwang, I. W.; Soci, C.; Moses, D.; Zhu, Z. G. D.; Waller, D.; Gaudiana, R.; Brabex, C. J.; Heeger, A. J. *Adv. Mater.* **2007**, *19*, 2307.
(79) Chekalin, S. V. *J. Exp. Theor. Phys.* **2006**, *103*, 756.
(80) Tkachenko, N. V.; Lemmetyinen, H.; Sonoda, J.; Ohkubo, K.; Sato, T.; Imahori, H.; Fukuzumi, S. *J. Phys. Chem. A* **2003**, *107*, 8834. Ramos, A. M.; Meskers, S. C. J.; van Hal, P. A.; Knol, J.; Hummelen, J. C.; Janssen, R. A. J. *J. Phys. Chem. A* **2003**, *107*, 9269.
(81) Sension, R. J.; Szarka, A. S.; Smith, G. R.; Hochstrasser, R. M. *Chem. Phys. Lett.* **1991**, *185*, 179.
(82) Ryasnyansky, A. I.; Ganeev, R. A.; Redkorechev, V. I.; Usmanov, T.; Priebe, G.; Fostiropoulos, K. *Fullerenes, Nanotubes, Carbon Nanostruct.* **2005**, *13*, 131.
(83) Kraabel, B.; Lee, C. H.; McBranch, D.; Moses, D.; Sariciftci, N. S.; Heeger, A. J. *Chem. Phys. Lett.* **1993**, *213*, 389.
(84) Thomas, T. N.; Taylor, R. A.; Ryan, J. F.; Mihailovič, D.; Zamboni, R. *Europhys. Lett.* **1994**, *25*, 403. Thomas, T. N.; Ryan, J. F.; Taylor, R. A.; Mihailovič, D.; Zamboni, R. *Int. J. Mod. Phys. B* **1992**, *6*, 3931.
(85) Hohmann, H.; Callegari, C.; Furrer, S.; Grosenick, D.; Campbell, E. E. B.; Hertel, I. V. *Phys. Rev. Lett.* **1994**, *73*, 1919.
(86) Yang, L.; Dorsinville, R.; Alfano, R. *Chem. Phys. Lett.* **1994**, *226*, 605.
(87) Couris, S.; Koudoumas, E.; Dong, F.; Leach, S. *J. Phys. B: At. Mol. Opt. Phys.* **1996**, *29*, 5033.
(88) Boucher, D.; Chekalin, S. V.; Kovalenko, S. A.; Matveets Yu, A.; Masselin, P.; Novikov, M. G.; Ragulsky, V. V.; Stepanov, A. G. *SPIE Proc.* **1997**, *3239*, 302.
(89) Farztdinov, V. M.; Dobryakov, A. L.; Ernsting, N. P.; Kovalenko, S. A.; Lozovik Yu, E.; Matveets, Yu. A *Laser Phys.* **1997**, *7*, 393. Farztdinov, V. M.; Kovalenko, S. A.; Matveets, Yu. A.; Starodubtsev, N. F.; Marowsky, G *Appl. Phys. B: Laser Opt.* **1998**, *66*, 225.
(90) Ishihara, S.; Ikemoto, I.; Suzuki, S.; Kikuchi, K.; Achiba, Y.; Kobayashi, T. *Chem. Phys. Lett.* **1998**, *295*, 475.
(91) Zhang, G. P.; Fu, R. T.; Sun, X.; Lin, D. L.; George, T. F. *Phys. Rev. B* **1994**, *50*, 11976.
(92) Buche, D.; Kovalenko, S. A.; Masselin, P.; Matveets, Yu. A.; Novikov, M. G.; Ragulsky, V. V.; Stephanov, A. G.; Chekalin, S. V. *Bull. Russ. Acad. Sci. Phys.* **1998**, *62*, 198.
(93) Sassara, A.; Zerza, G.; Chergui, M.; Ciulin, V.; Ganiére, J.-D.; Deveaud, B. *J. Chem. Phys.* **1999**, *111*, 689.
(94) van Hal, P. A.; Janssen, R. A. J.; Lanzani, G.; Cerullo, G.; Zavelani-Rossi, M.; De Silvestri, S. *Chem. Phys. Lett.* **2001**, *345*, 33.
(95) Stepanov, A. G.; Portella-Oberli, M. T.; Sassara, A.; Chergui, M. *Chem. Phys. Lett.* **2002**, *358*, 516.
(96) Bhardwaj, V. R.; Corkum, P. B.; Rayner, D. M. *Phys. Rev. Lett.* **2004**, *93*, 043001.
(97) Berera, R.; Moore, G. F.; van Stokkum, I. H. M.; Kodis, G.; Liddell, P. A.; Gervaldo, M.; van Grondelle, R.; Kennis, J. T. M.; Gust, D.; Moore, T. A.; Moore, A. L. *Photochem. Photobiol. Sci.* **2006**, *5*, 142.
(98) Manzoni, C.; Polli, D.; Cerullo, G. *Rev. Sci. Instrum.* **2006**, *77*, 023103.
(99) Shchatsinin, I.; Laarmann, T.; Stibenz, G.; Steinmeyer, G.; Stalmashonak, A.; Zhavoronkov, N.; Schulz, C. P.; Hertel, I. V. *J. Chem. Phys.* **2006**, *125*, 194320.
(100) Laarmann, T.; Schchatsinin, I.; Stalmashonak, A.; Boyle, M.; Zhavoronkov, N.; Handt, J.; Schmidt, R.; Schulz, C. P.; Hertel, I. V. *Phys. Rev. Lett.* **2007**, *98*, 058302.
(101) Zhang, G. P.; Sun, X.; George, T. F. *Phys. Rev. B* **2003**, *68*, 165410.
(102) Toivonen, T. L. J.; Hukka, T. I. *Chem. Phys. Lett.* **2008**, *421*, 243.
(103) Jones, G. A.; Acocella, A.; Zerbetto, F. *Theor. Chem. Acc.* **2007**, *118*, 99.
(104) Su, W. P.; Schrieffer, J. R. *Proc. Natl. Acad. Sci. (USA)* **1980**, *77*, 5626.
(105) Nakamura, A.; Ichida, M.; Yajima, T. *Prog. Cryst. Growth Charact. Mater.* **1996**, *33*, 169.

(106) Sun, X.; Zhang, G. P.; Ma, Y. S.; Lee, K. H.; Park, T. Y.; George, T. F.; Pandey, L. N. *Phys. Rev. B* **1996**, *53*, 15481.

(107) Bruening, J.; Friedman, B. *J. Chem. Phys.* **1997**, *106*, 9634.

(108) Zhang, G. P.; Sun, X.; George, T. F.; Pandey, L. N *J. Chem. Phys.* **1997**, *106*, 6398. Zhang, G. P.; Zong, X. F.; Sun, X.; George, T. F.; Pandey, L. N. *Phys. Lett. A* **1996**, *220*, 275.

(109) You, W. M.; Wang, C. L.; Zhang, F. C.; Su, Z. B. *Phys. Rev. B* **1993**, *47*, 4765.

(110) Zhang, G. P.; George, T. F. *Phys. Rev. B* **2002**, *66*, 033110.

(111) Boyle, M.; Hedén, M.; Schulz, C. P.; Campbell, E. E. B.; Hertel, I. V. *Phys. Rev. A* **2004**, *70*, 051201.

(112) Boyle, M.; Laarmann, T.; Hoffmann, K.; Hed, M.; Campbell, E. E. G.; Schulz, C. P.; Hertel, I. V. *Eur. Phys. J. D* **2005**, *36*, 339.

(113) Zhang, G. P.; George, T. F. *Phys. Rev. Lett.* **2004**, *93*, 147401.

(114) Torralva, B.; Niehaus, T. A.; Elstner, M.; Suhai, S.; Frauenheim, Th.; Allen, R. E. *Phys. Rev. B* **2001**, *64*, 153105.

(115) Liu, Z.-D.; Zeng, L.; Zhu, S.-Y.; George, T. F. *J. Mod. Opt.* **1998**, *45*, 2473. DeVries, P. L.; Lam, K. S.; George, T. F. *Int. J. Quantum Chem.: Quantum Chem. Symp.* **1979**, *13*, 541.

(116) Zhang, G. P.; George, T. F. *Phys. Rev. B* **2007**, *76*, 085410.

(117) Zhang, G. P. *Phys. Rev. Lett.* **2003**, *91*, 176801.

(118) Bauer, D.; Ceccherini, F.; Macchi, A.; Cornolti, F. *Phys. Rev. A* **2001**, *64*, 063203.

(119) Zhang, G. P. *Phys. Rev. Lett.* **2005**, *95*, 047401.

(120) Zhang, G. P.; George, T. F. *Phys. Rev. A.* **2006**, *74*, 023811. Zhang, G. P. *Int. J. Mod. Phys. B* **2007**, *21*, 5167. Zhang, G. P.; George, T. F. *J. Opt. Soc. Am. B* **2007**, *24*, 1150.

(121) Brorson, S. D.; Kelly, M. K.; Wenschuh, U.; Buhleier, R.; Kuhl, J. *Phys. Rev. B* **1992**, *46*, 7329.

(122) Fleischer, S. B.; Ippen, E. P.; Dresselhaus, G.; Dresselhaus, M. S.; Rao, A. M.; Zhou, P.; Eklund, P. C. *Appl. Phys. Lett.* **1993**, *62*, 3241.

(123) Fleischer, S. B.; Pevzner, B.; Dougherty, D. J.; Zeiger, H. J.; Dresselhaus, G.; Dresselhaus, M. S.; Ippen, E. P.; Hebard, A. F. *Appl. Phys. Lett.* **1997**, *71*, 2734.

(124) Fleischer, S. B.; Pevzner, B.; Dougherty, D. J.; Zeiger, H. J.; Dresselhaus, G.; Dresselhaus, M. S.; Ippen, E. P.; Hebard, A. F. *Phys. Rev. B* **2000**, *62*, 1366.

(125) Allen, P. B. *Phys. Rev. Lett.* **1987**, *59*, 1460.

(126) Kabanov, V. V.; Demsar, J.; Podobnik, B.; Mihailovič, D. *Phys. Rev. B* **1999**, *59*, 1497. Demsar, J.; Averitt, R. D.; Taylor, A. J.; Kabanov, V. V.; Kang, W. N.; Kim, H. J.; Choi, E. M.; Lee, S. I. *Phys. Rev. Lett.* **2003**, *91*, 267002. Gedik, N.; Orenstein, J.; Liang, R.; Bonn, D. A.; Hardy, W. N. *Science* **2003**, *300*, 1410.

(127) Zhang, G. P.; George, T. F. *Phys. Rev. B* **2006**, *73*, 035422.

(128) Kuhnke, K.; Becker, R.; Berger, H.; Kern, K. *J. Appl. Phys.* **1996**, *79*, 3781. Kuhnke, K.; Epple, M.; Kern, K. *Chem. Phys. Lett.* **1998**, *294*, 241.

(129) Koopmans, B.; Janner, A.-M.; Jonkman, H. T.; Sawatzky, G. A.; van der Woude, F. *Phys. Rev. Lett.* **1993**, *71*, 3569.

(130) Barbour, L. W.; Hegadorn, M.; Asbury, J. B. *J. Am. Chem. Soc.* **2007**, *129*, 15884. Schuster, D. I.; Li, K.; Guldi, D. M.; Palkar, A.; Echegoyen, L.; Stanisky, C.; Cross, R. J.; Niemi, M.; Tkachenko, N. V.; Lemmetyinen, H. *J. Am. Chem. Soc.* **2007**, *129*, 15973.

(131) Lioudakis, E.; Othonos, A.; Alexandrou, I.; Hayashi, Y. *Appl. Phys. Lett.* **2007**, *91*, 111117.

(132) Hwang, I. W.; Moses, D.; Heeger, A. J. *J. Phys. Chem. C* **2008**, *112*, 4350.

JP802244B